– 1 –

The Particulate Phase: A Voyage from the Molecule to the Granule

Flow behavior of solid–liquid two-phase flow systems depends on the properties of the dispersed solid phase, the continuous liquid phase that suspends the solids and the interactions between the two phases. This chapter is an overview of molecular interactions leading up to the formation of solid particle aggregates and surface forces responsible for the stability of suspensions.

1.1 MOLECULAR INTERACTIONS

Molecules of all matter at a temperature above absolute zero possess internal energy expressed as motion in the form of rotation, vibration, and translation, provided there is enough space to permit these motions. Because of the random translatory motion, the molecules frequently collide with each other. The statistical average distance traveled between two collisions is called the mean free path. When the energies of the colliding molecules are not "high enough" to end-up in a coalition, the original molecules keep colliding with other molecules on their paths, their energies being redistributed after each collision. This random motion, called Brownian motion, is expressed as thermal energy in the terms of $k_B T$, where k_B is the Boltzmann constant [$1.381 \times 10^{-23} \mathrm{J\,K^{-1}}$] and T, the absolute temperature in [K]. All the molecules would be free and would move randomly within the medium, if thermal energy or internal energy were the only sources of energy the molecules possess. If there is any aggregation or some kind of an order between the molecules, it is due to the attractive forces existing between the molecules. For the attractive forces to be effective, the potential energy they generate should be equal or greater in magnitude than the thermal energy. The thermal energy at 25°C amounts to $1.381 \times 10^{-23} \times 298 = 4.12 \times 10^{-21}$ J, so bonds with energies less than this are bound to break up at 25°C.

All the interactions between atoms and simple molecules are essentially electrostatic in origin. This stems up from the structure of the atom: A positively charged nucleus surrounded by a negatively charged electron cloud. The electron density in between atoms of equal electronegativity, making up a molecule is symmetrical. If there is a deficiency of electrons in this cloud in comparison with a neutral atom or a molecule, the molecule

attains a positive charge, called a cation. If, on the other hand, there is a surplus of electrons, the molecule becomes negatively charged and is called an anion. Two similarly charged ions repel and dissimilar ions attract each other. The ionic charge Q of the ionic molecule is the product of the number of missing/surplus electrons, the valence z_i, and the charge of a single electron e in Coulombs, $e = 1.602 \times 10^{-19}$ C, $Q = z_i\, e$. Due to the symmetry of the electron cloud, the electric field, E, around an ion is considered to have spherical symmetry and to decrease with the square of the radial distance r:

$$E = \frac{Q / \varepsilon_0 \varepsilon_\mathrm{r}}{4\pi r^2} = \frac{z_i e / \varepsilon_0 \varepsilon_\mathrm{r}}{4\pi r^2} \tag{1.1}$$

Charge alone does not determine the electric field; the electrical permittivity of vacuum, ε_0 [$\varepsilon_0 = 8.854 \times 10^{-12}\ \mathrm{C^2\ J^{-1} m^{-1}}$], and the relative permittivity with respect to vacuum of the medium in which the charged ions exist, ε_r, determine the effective charge around which the field is set up. If an ion of charge Q_2 is brought into the electrical field of another ion, E, it acquires potential energy given by

$$U_{\mathrm{ion-ion}} = \frac{Q_1 Q_2}{4\pi\varepsilon_0 \varepsilon_\mathrm{r} r} = \frac{z_1 z_2 e^2}{4\pi\varepsilon_0 \varepsilon_\mathrm{r} r} \tag{1.2}$$

The potential energy U is positive if the charges are similar, and negative if they are not. The interaction force, F, is the negative of the derivative of the potential energy with respect to r, the distance between the central Q_1 and the incoming Q_2 charges

$$F = -\nabla U_{\mathrm{ion-ion}} = \frac{Q_1 Q_2}{4\pi\varepsilon_0 \varepsilon_\mathrm{r} r^2} = \frac{z_1 z_2 e^2}{4\pi\varepsilon_0 \varepsilon_\mathrm{r} r^2} \tag{1.3}$$

If the charges Q_1 and Q_2 are similar, the ions repel each other, both the potential and the force being positive. Unlike charges attract each other and are denoted by a negative force and potential. Since this force of attraction or repulsion is much larger than $k_\mathrm{B}T$, the interaction is not affected by random molecular motions in the temperature range of solutions or suspensions under ordinary conditions.

The basic assumption of these equations is that the ions act like point sources and do not disturb the electron density distribution of each other. When the molecules are composed of atoms with different electronegativity, the electron distribution departs from symmetrical in favor of the more electronegative component. The electronegative atom acquires a slightly negative charge, while the other atom or group of atoms, a slightly positive charge: The molecule acts like a rod with different charges at either end. When such a dipole enters into the electric field of an ion, the ion attracts the end carrying the opposite charge and repels the other end. This dual interaction causes the dipole to rotate within the electric field of the ion to orient itself with respect to the other ion and monoatom–diatom transition takes place. The charge on a dipole is denoted by the dipole moment, m, the product of the charge on one of the poles and the length l of the molecule in between the two charged ends.

$$m = Q^+ l = Q^- l \tag{1.4}$$

Even though the origin of the charge is not due to deficiency or excess of electrons, dipoles also interact like ions with the charge Q_i replaced by the dipole moment, m (Stokes and Evans, 1997). In this way, the potential energy between a dipole and an ion, a distance r apart is given by

$$U_{\text{ion-dip}} = -\frac{Q_i m \cos\theta}{4\pi\varepsilon_0\varepsilon_r r^2} \tag{1.5}$$

θ is the angle between the axis of the dipole and the line joining the centers of the ion and the dipole. Cosθ term takes into account the interaction of both the positive and the negative ends of the dipole with the ion. For a cation, z_i is positive and the maximum interactions (attraction and repulsion in sequence) occur when the angle is a multiple of π radians and the axis of the dipole is congruent with the line joining the centers. For this same reason, a sphere of dipoles oriented radially toward the ion surrounds an ion in solution in a polar compound, such as water.

Dipoles also interact with each other. Since the potential created by the dipoles is not as strong as that of the ions, the dipoles are free to rotate. Hence, the potential energy between the dipoles is a function of distance r between their centers, as well as the angles in θ and ϕ directions between their axes in spherical coordinates. Through trigonometric calculations, the potential between the two dipoles is obtained with an equation similar to eq. (1.5)

$$U(r,\theta_1,\theta_2,\phi) = -\frac{m_1 m_2}{4\pi\varepsilon_0\varepsilon_r r^3}(2\cos\theta_1\cos\theta_2 - \sin\theta_1\sin\theta_2\cos\phi) \tag{1.6}$$

To take into account all possible orientations of the dipoles, the angle average of the potential energy is taken through the use of Boltzmann distribution

$$x_i = e^{-(U_i/k_B T)} \tag{1.7}$$

which gives the fraction of the ions x_i that possess a given potential energy, U_i, to the disturbing thermal energy, $k_B T$, ratio. The free rotation of the dipoles signifies that their thermal energy is greater than their interaction potential, $U(r, \theta, \phi) < k_B T$. The exponential term can then be expanded and integrated

$$U(r) = \frac{\int U(r,\theta,\phi)\exp(-U(r,\theta,\phi)/k_B T)\sin\theta\, d\theta\, d\phi}{\int_0^{2\pi}\int_0^{2\pi}\sin\theta\, d\theta\, d\phi} \tag{1.8}$$

to give the angle-averaged potential between two dipoles, known as the *Keesom* interaction

$$U_{\text{dip-dip}} = -\frac{2m_1^2 m_2^2}{3(4\pi\varepsilon_0\varepsilon_r)^2 k_B T r^6} \text{ for } k_B T > \frac{m_1 m_2}{4\pi\varepsilon_0\varepsilon_r r^3} \tag{1.9}$$

This angle-averaged interaction potential between two dipoles is always attractive (due to the negative sign) and is the only interaction dependent on temperature, decreasing as the temperature increases.

Dipoles, when close enough to another molecule, perturb their electronic cloud and cause a redistribution of electrons opposite to their own. This redistribution shifts the charge center of the molecule from the positively charged nucleus, generating a restoring force, analogous to Hooke's law, which counteracts the attractive force of the electric field of the dipole. The total potential created between the permanent and induced dipoles is the sum of the attractive and restoring forces, given in terms of polarization coefficient, α

$$U = -\frac{1}{2}\alpha E^2 = -\frac{1}{2}(\alpha E)(E) \tag{1.10}$$

as one half the potential between a dipole and an ion of electric fields αE and E, respectively. The full potential energy cannot be used in the case of induced dipoles because half the potential energy is expended during the inducement, in the displacement of the electron cloud from its original distribution. The electric field to which the polarized molecule is subjected to is dependent on the angle between the permanent and induced dipole, θ, and the distance between their centers, r

$$E(r,\theta) = \frac{m(1+3\cos^2\theta)^{1/2}}{4\pi\varepsilon_0\varepsilon_r r^3} \tag{1.11}$$

where m is the dipole moment of the polar molecule. Replacing this expression for E in eq. (1.10) and angle averaging the resultant equation gives

$$U_{\text{dip-ind dip}} = -\frac{m_1^2\alpha_2 + m_2^2\alpha_1}{(4\pi\varepsilon_0\varepsilon_r)^2 r^6} \tag{1.12}$$

where the subscripts 1 and 2 refer to permanent and induced dipoles. This equation is known as the *Debye* interaction potential which is always attractive.

The induced dipole in turn, induces a dipole in an adjacent molecule. The interaction potential derived theoretically from the Schrödinger equation is known as the *London* potential

$$U_{\text{ind dip-ind dip}} = -\frac{3}{2}\frac{\alpha_1\alpha_2}{(4\pi\varepsilon_0\varepsilon_r)^2 r^6}\left(\frac{\hbar v_1 v_2}{v_1 + v_2}\right) \tag{1.13}$$

In this equation, $\hbar$ is the Planck constant [$\hbar = 6.626 \times 10^{-34}$ Jsec], v the characteristic vibrational frequency of electrons [sec^{-1}], and their product $\hbar v$ the ionization energy of the atoms.

1.1.1 Attractive forces among molecules

Attractive forces among molecules are classically grouped as electrostatic or electrodynamic in origin. Ions with opposing electrostatic charges create a potential given by eq. (1.2) and

attract each other with a force given by eq. (1.3). The attractions between ions and permanent dipoles also belong to this group, the potential or the free energy of interaction given by eq. (1.5). It should be noted that the free energy of interaction of ion–ion interactions vary inversely with the distance in between the ions while that of ion–dipole interactions vary with the square of the distance. This means that these forces are effective over long distances of separation of the molecules.

van der Waals attractions

The interaction potential between permanent dipoles, the *Keesom* equation (eq. (1.9)), between permanent and induced dipoles, the *Debye* equation (eq. (1.12)), and between induced dipoles, *London* equation (eq. (1.13)) are collectively known as *van der Waals attractions*. These forces originate from the asymmetry in the distribution of electrons within the molecules and are created by induction of a polar or an induced-polar molecule in close proximity in the process of constant rotational and translational motion. So, these forces are dynamic in origin and are short-range attractive forces as shown by the r^{-6} dependence in each case. Keesom interactions are effective in the alignment of polar molecules; on the other hand, the London interactions are effective among all types of molecules and mainly responsible for the attraction of particles as will be shown in the next section.

1.1.2 Repulsive forces among molecules

Like attractive forces, repulsive forces also arise between ions carrying similar charges and dipoles the magnitudes of which are calculated with the same equations. Due to the similarity of the charges, both the force and the potential energy are always positive.

Apart from these forces of electrostatic origin, repulsion can also arise due to overlapping of electron clouds, at extremely short distances. The potential energy that arises due to repulsive interaction of electron clouds are given by the general expression

$$U(r) = \left(\frac{\sigma}{r}\right)^n \tag{1.14}$$

σ is related to the size of the molecule defined by the very short-range steric repulsive forces that determine the identity of the molecule by setting the limits of closest approach. r is the distance between the "closest-approach boundaries" of the atoms. In the hard-sphere concept of the molecule, the exponent n is taken as $n = \infty$. In such a case, the potential energy is either zero, when $r \gg 0$, or goes to infinity when $r \ll 0$. Generally, the electron clouds show a limited flexibility, so the Lennard–Jones potential is the most widely used potential energy expression

$$U(r) = -\frac{A_{LJ}}{r^6} + \frac{B_{LJ}}{r^{12}} \tag{1.15}$$

The first term on the right hand side (RHS) that shows a 6th power variation with distance separating the molecules signifies the three van der Waals attractions and the second term,

with the 12th power variation signifies the repulsion due to the close approach of the electron clouds. A_{LJ} and B_{LJ} are adjustable constants related with the size of the molecules.

1.2 INTERACTIONS OF ELECTRICAL ORIGIN BETWEEN PARTICLES

The same forces that exist between a pair of molecules also exist between a great number of molecules aggregated in the form of a particle. The interactions may be attractive based on electronic distributions (van der Waals) or repulsive due to ionic distributions (double layer repulsions).

1.2.1 Attractions between particles

If the particles are not ionic, and have a uniform distribution of molecules, one of the components of the van der Waals forces will be effective in forming attractive forces between the particles. Assuming each molecule in one particle to interact with a molecule on another particle and that, these interactions can be added pair wise, attractive forces between two bodies can be calculated. In the original derivation of Hamaker (1937), the number distribution of molecules in a differential volume element is taken and the potential energy between the molecules of the control element and a single molecule is calculated (Stokes and Evans, 1997). The general form of the van der Waals interaction potential can be written as

$$U(r) = -\frac{A_{LJ}}{r^6} \tag{1.16}$$

All the molecules in the differential volume dv, $(\rho N_A/M)dv$, will interact with this single molecule, that is situated at a normal distance along the axis in cylindrical coordinates, causing the evolution of a potential

$$U(h) = -\int_{\upsilon} A_{LJ}\left(\frac{\rho N_A}{M}\right)d\upsilon = -A_{LJ}\left(\frac{\rho N_A}{M}\right)\left(\frac{\pi}{6h^3}\right) \tag{1.17}$$

where ρ is the density of the particle, N_A the Avogadro number [6.023×10^{23} molecules per mol], and M the molecular weight. If this single molecule is one of the many in another particle, then the potential due to all the molecules per unit area [J m^{-2}] facing the first particle ($(\rho N_A/M)dh$) would be

$$U(h) = -\int_{h}^{\infty} A_{LJ}\left(\frac{\rho N_A}{M}\right)^2 \frac{\pi}{6}\frac{dh}{h^3} = -A_{LJ}\left(\frac{\rho N_A}{M}\right)^2 \frac{\pi}{12h^2} \tag{1.18}$$

The integration limits in eq. (1.18) is the distance between the parallel plates, h, and the other end of the planar particle that is at a very large distance approaching infinity, in terms of the attraction range. The result turns out to be inversely proportional to the square of the distance separating the particles, which can be classified as long-range interaction. The coefficient of the interaction potential A_{LJ} and the term related with the number of

molecules are collected in a single parameter, which is a material constant called the *Hamaker constant*, H.

$$H_{11} = A_{\mathrm{LJ}} \left(\frac{\rho N_{\mathrm{A}} \pi}{M} \right)^2 \tag{1.19}$$

The attractive interaction potential between two flat plates in vacuum is given as

$$U(h) = -\frac{H_{11}}{12\pi h^2} \tag{1.20}$$

As only the particle–particle interactions are considered in the derivation, it is denoted by the symbol, H_{11}, where the subscript 1 indicates that the two particles are made of the same material. The most general attractive force effective between all types of molecules is the dispersion or the London forces between two induced dipoles. For particles composed of identical particles, eq. (1.13) is reduced to

$$U(r) = -\frac{3}{4} \frac{\alpha^2 \hbar v}{(4\pi\varepsilon_0)^2 r^6} \tag{1.21}$$

and the Hamaker constant for the two particles interacting in vacuum becomes

$$H_{11} = \frac{3}{4} \left(\frac{\rho N_{\mathrm{A}} \pi}{M} \right)^2 \frac{\alpha^2 \hbar v}{(4\pi\varepsilon_0)^2} \tag{1.22}$$

If the particles are suspended in a liquid medium, the attractive potential is greatly reduced due to the intervening medium. Denoting the intervening liquid with the subscript 2, the Hamaker constant would be denoted by H_{121}, approximated as

$$H_{121} = (H_{11}^{1/2} - H_{22}^{1/2})^2 \tag{1.23}$$

Water as the most frequently suspending agent has a Hamaker constant of $H_{22} = 3.7 \times 10^{-20}$ J. If the two particles are not identical in properties, the interactions between the first particle 1 and the medium 2, as well as the second particle 3 and the medium 2 should be taken into account, approximated by the expression

$$H_{123} = (H_{11}^{1/2} - H_{22}^{1/2})(H_{33}^{1/2} - H_{22}^{1/2}) \tag{1.24}$$

Eq. (1.23) is always positive due to the squared term, so unless the Hamaker constant in vacuum of the suspending medium is equal to that of the particles, the two particles will always attract each other. Naturally when H_{121} equals zero, the particles will be inert toward each other. When two dissimilar particles are under consideration, the value of the Hamaker constant of the medium becomes important: If H_{22} is in between H_{11} and H_{33} in value then H_{123} in eq. (1.24) will be negative and the particles will repel each other leading onto a stable suspension.

An expression similar to eq. (1.20) for planar particles is derived for spherical particles by using the Derjaguin approximation (Stokes and Evans, 1997), assuming the surface of the sphere is made up of an infinite number of planar steps. Applying the equation for planar surfaces to each vertical surface of the step and integrating over the surface of the particle, gives the interaction potential between two spheres of equal radii R as

$$U(h)_{\text{sphere}} = -\frac{H_{11}R}{12h}, \quad R \gg h \tag{1.25}$$

and for spheres of unequal radii R_1 and R_3 at a distance h much smaller than the radius of either particle

$$U(h) = -\frac{H_{13}R_1R_3}{6h(R_1 + R_3)} \tag{1.26}$$

In both cases, the potential changes inversely with the distance separating the spherical particles and the attractive force, equal to the derivative of the potential, changes with the square of the distance.

If the particles were suspended in a liquid medium, eq. (1.20) for flat plates, eqs. (1.25) and (1.26) for spheres would be

$$U(h)_{\text{plate}} = -\frac{H_{121}}{12\pi h^2} \tag{1.20a}$$

$$U(h)_{\text{sphere}} = -\frac{H_{121}R}{12h}, \quad R \gg h \tag{1.25a}$$

$$U(h)_{\text{sphere}} = -\frac{H_{123}\,R_1R_3}{6h(R_1 + R_3)} \tag{1.26a}$$

In the above derivation originally made by Hamaker in 1937, the sum of all the pair-wise interactions among the molecules or atoms in a particle were taken into account. Hamaker constant is a material constant of the interacting particles and the medium within which they are suspended in terms of polarizabilities and number densities of the molecules making up the particles, as given in eq. (1.22). In the more rigorous treatment of Lifshitz (1956), instead of being considered in terms of their component molecules, the particles are taken as a continuum with given dielectric properties. van der Waals interaction is the result of fluctuations in the electromagnetic field between the two particles, modified by the intervening suspension medium. Hamaker constant can be estimated from knowledge of frequency-dependent dielectric properties of the interacting materials together with the intervening medium and the geometry of the particles. Accuracy of the Hamaker constant is related to the precision and accuracy of dielectric spectra and mathematical representation of the data. Bergstrom (1997) has critically evaluated the available optical data in the

Table 1.1

Hamaker constants

Material	Crystal structure	Hamaker constant $\times 10^{20}$ J	
		In vacuum	In water
α-Al_2O_3	Hexagonal	15.2	3.67
PbS	Cubic	8.17	4.98
SiO_2 (quartz)	Trigonal	8.86	1.02
SiO_2 (silica)	Amorphous	6.50	0.46
TiO_2	Tetragonal	15.3	5.35
ZnO	Hexagonal	9.21	1.89
ZnS	Cubic	15.2	4.80
ZnS	Hexagonal	17.2	5.74

Source: With permission of Elsevier Science Ltd.

literature and calculated the Hamaker constant by the full Lifshitz method. Table 1.1 is abridged from the results of Bergstrom.

1.2.2 Ionic interactions between charged surfaces

Particle surfaces in a liquid medium acquire surface charge either through dissolution and diffusion of ions of the particle from the surface into the solution leaving the particle surfaces in an ionized state, or through adsorption of ions from solution onto the particle surface. If in addition, the suspension medium is an electrolyte solution, then ions of the solution will interact with the ions on the surface of the particle. If the ionization or adsorption sites are uniformly distributed over the surface, the charge concentration on the particle surface can be quantified in terms of surface charge density, σ_0 [Cm^{-2}]. In the solution side of the solid/liquid interface, ions of opposite charge will accumulate nearby the surface to maintain electrical neutrality. The charge density in solution ($z_i e C_{iN}$), will increase as the particle surface is approached. A potential, Φ, will then be created between the surface of the particles and the ions in solution that have accumulated near the particle. The charge density in solution is proportional to the potential gradient, in accordance with the Poisson equation

$$\nabla^2 \Phi = -\frac{1}{\varepsilon_r \varepsilon_0} \sum_i z_i e C_{iN} \tag{1.27}$$

where C_{iN} is the number concentration. The proportionality constant, the inverse of the permittivity or the dielectric constant of the solution, $\varepsilon_r \varepsilon_0$, takes into account the van der Waals interactions among the molecules of the solution, so that only the ions are taken into consideration. The concentration term C_{iN} in the expression giving the charge density of the solution is the number of ions per unit volume [m^{-3}] of the solution. These ions have sufficient potential energy to overcome the dispersive thermal or internal energy ($k_B T$) to

gather around the particle, instead of being uniformly distributed in random in the solution. So the Boltzmann distribution, analogous to eq. (1.7) can be used to relate the fraction of ions in solution with the potential created by the particle Φ

$$x_i = \frac{C_{iN}}{C_{iN}^0} = \exp\left(-\frac{z_i e \Phi}{k_B T}\right) \tag{1.28}$$

where C_{iN}^0 is the concentration when there is no potential ($\Phi = 0$). Replacing eq. (1.28) into eq. (1.27), Poisson–Boltzmann equation is obtained which relates the potential gradient with the concentration of ions in solution.

$$\nabla^2 \Phi = -\frac{1}{\varepsilon_r \varepsilon_0} \sum_i z_i e C_{iN}^0 \exp\left(-\frac{z_i e \Phi}{k_B T}\right) \tag{1.29}$$

Assuming the particles as flat flakes with surfaces exposed to the solution in one direction only, eq. (1.29) is solved to give the Gouy–Chapman relation, valid for symmetrical electrolytes containing equal numbers of cations and anions in a molecule (Stokes and Evans, 1997)

$$\Phi(h) = \frac{2k_B T}{ze} \ln\left(\frac{1 + \Gamma_0 \exp(-\kappa h)}{1 - \Gamma_0 \exp(-\kappa h)}\right) \tag{1.30}$$

The potential Φ is given implicitly in terms of the Boltzmann distribution in the Γ_0 term as

$$\Gamma_0 = \frac{\exp(ze\Phi_0 / 2k_B T) - 1}{\exp(ze\Phi_0 / 2k_B T) + 1} \tag{1.31}$$

In eq. (1.30), h is the distance from the particle surface and κ the gradient of the potential near the surface. From dimensional analysis, κ must have the dimension of inverse length [L^{-1}]. κ^{-1} is called the *Debye screening length*.

It should be noted that eqs. (1.30) and (1.31) relate the potential Φ created by the charged particle to the charge distribution in the solution. On the ground that electrical neutrality should be maintained within the particulate suspension, the total charge on the particle surfaces should be neutralized by the opposite charged ions in the solution. Stokes and Evans (1997) related the potential Φ to the charge density on the surface of the particle, σ_0, using the Poisson–Boltzmann relation

$$\sigma_0 = (2\varepsilon_r \varepsilon_0 k_B T C_{iN}^0)^{1/2} \left[\exp\left(\frac{z_i e \Phi_0}{2k_B T}\right) - \exp\left(-\frac{z_i e \Phi_0}{2k_B T}\right)\right] \tag{1.32}$$

The concepts and the effect of different parameters introduced so far are illustrated schematically in Figure 1.1. The potential decreases steeply with distance from the solid surface as the ionic concentration increases as shown in the left hand side (LHS) of the plate corresponding to Figure 1.1(a), in accordance with eq. (1.29). The effect of the

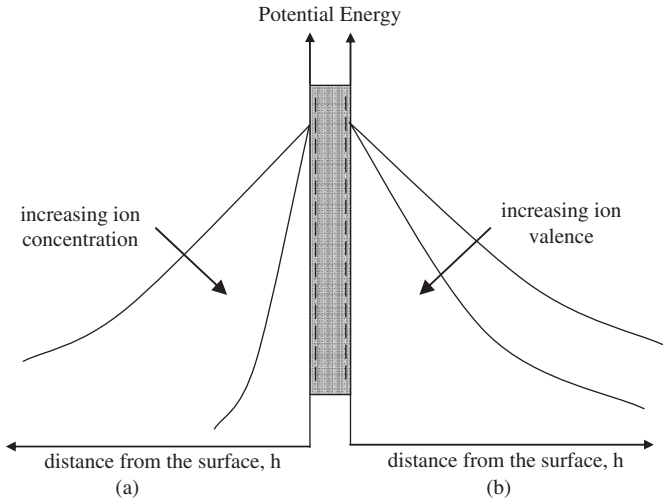

Figure 1.1 Effect of (a) ion concentration (b) ion valence (1:1 (NaCl), 2:2 ($ZnSO_4$)) on the potential as a function of distance from the surface.

valence number in symmetrical electrolytes containing equal numbers of cations and anions in a molecule are shown on the RHS of the plate corresponding to Figure 1.1(b). Higher valence (2:2) causes a steeper decline of the potential with distance from the surface according to eq. (1.30).

The distribution of ions around a particle is given in Figure 1.2(a), in an exaggerated scale to show the different layers. The ions of the particle are shown as being homogeneously distributed over the surface area. A layer of ions of opposite charge adjacent to the particle is called the *Stern layer*. As the Debye length, designated as κ^{-1}, is an imaginary layer without a physical existence, it is arbitrarily shown to be several atomic diameters in thickness. The Debye length is defined by the simplified solution (Stokes and Evans, 1997) of the Poisson–Boltzmann equation valid for $ze\Phi \ll k_B T$ as

$$\Phi(h) = \Phi_0 \exp(-\kappa h) \tag{1.33}$$

Debye length is defined as the distance from the surface ($h = 1/\kappa$), where the electrical potential decreases to 37% of its value at the particle surface:

$$\frac{\Phi}{\Phi_0} = e^{-1} = 0.37 \tag{1.33a}$$

and changes parametrically with the electrolyte concentration and charge, permittivity of the medium and temperature according to eq. (1.34)

$$\frac{1}{\kappa} = \left[\frac{\varepsilon_r \varepsilon_0 k_B T}{\Sigma (z_i e)^2 C_{iN}^0} \right]^{1/2} \tag{1.34}$$

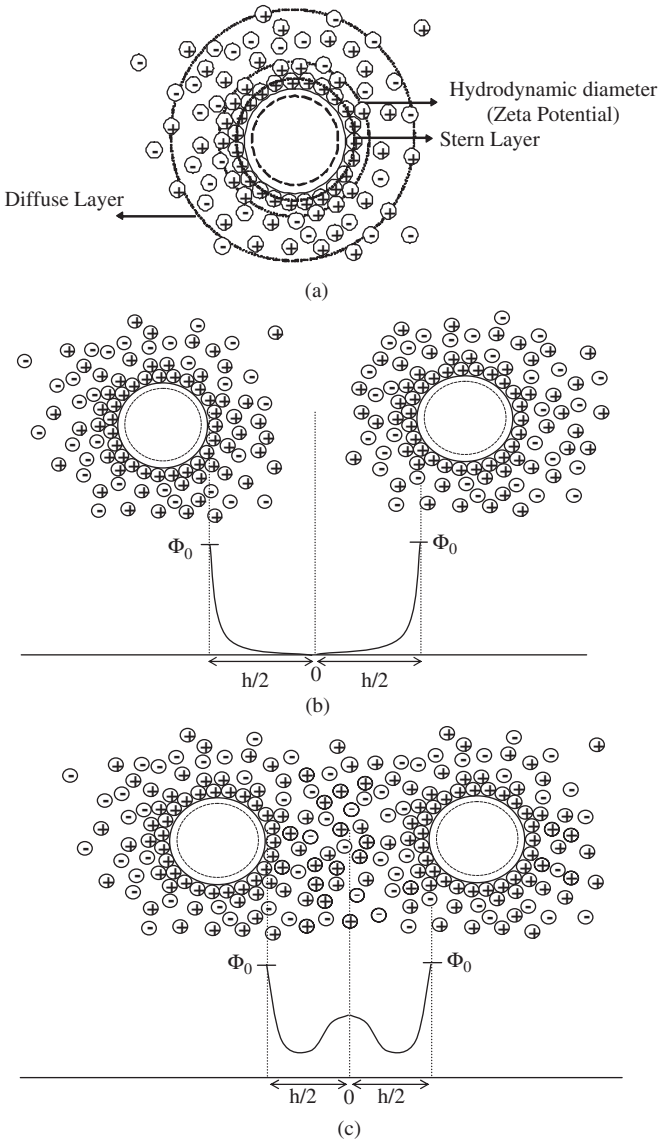

Figure 1.2 Distribution of counterions around charged particles. (a) Various layers defined within the diffuse ions. (b) Variation of electrical potential between two approaching ions. (c) Potential increase due to overlap of diffuse ions on close approach of the particles.

A decrease in Debye length, κ^{-1}, signifies closer approach of the particles, and in the limit, one of the particles being entrapped in the secondary or primary energy minimum of the other, leading on to coagulation, as will be explained in the following sections. Concentration of electrolytes in solution, C_{iN}^0, should be increased if coagulation is desired to take place among the particles. Debye length varies inversely with the square of the

valence of the ions. For this reason, multivalent ions with $z_i > 1$ are able to approach very closely to charged surfaces. This effect has a bearing in many important cases such as in the aggregation of red blood cells (RBCs), and the production of metal oxides in microemulsions, where the metal ion is situated very close to the hydrophilic heads of the anionic surfactants, making up the inner surface of the micelles that serve as nanoreactors.

Zeta potential is the only experimentally measurable length scale in the ionic diffuse layer that can be measured with electrophoresis. The method is based on the calculation of the particle diameter based on the diffusion rate of the particle in an electric field. The hydrodynamic diameter, d_h, includes not only the particle diameter itself but also the Stern layer and a portion of the diffuse layer; i.e., the ions on which the effect of attractive forces of electrostatic origin are greater than the hydrodynamic shear forces acting on the particle during its travel.

Hitherto, the charged molecules were simply referred to as "ions" without regard to their interactions with the particles. The ions can be classified into three groups in terms of their effect on the particle: Indifferent ions, potential determining ions, and charge reversing ions.

Indifferent ions do not affect the potential or the charge distribution on the particle surface; they affect the Gouy–Chapman diffuse layer of ions surrounding the particle. An increase in the concentration of indifferent ions in the suspension medium causes a decrease in the Debye length, permitting closer approach of the charged particles, eventually leading up to coagulation. Generally, sodium chloride (NaCl) is used to bring about the indifferent electrolyte effect.

Potential determining ions change the surface potential Φ_0 of the particle when adsorbed on the surface. If the particles are ionic, such as metal salts or metal hydroxides, then the potential of the ions in solution and those adsorbed on the surface are equal according to the Gibbs adsorption isotherm ($\mu_{EC}^{sol} = \mu_{EC}^{surf}$). μ_{EC} includes both the electrical and chemical effects (Reid, 1990)

$$(z_i F\Phi_i + \mu_0 + k_B T \ln a_i)^{surf} = (z_i F\Phi_i + \mu_0 + k_B T \ln a_i)^{sol} \tag{1.35}$$

Rearrangement of eq. (1.35) gives

$$\Phi_i^{surf} - \Phi_i^{sol} = \left(\frac{k_B T \ln (a_i^{sol} / a_i^{surf})}{z_i F} \right) = \left(\frac{k_B T}{z_i F} \ln a_i^{sol} - \frac{k_B T}{z_i F} \ln a_i^{surf} \right) \tag{1.36}$$

where a_i is the activity, F the Faraday constant [9.648×10^4 C mol^{-1}], z_i the valence of the ion, and $\Phi_i^{surf} - \Phi_i^{sol}$ the electrical surface potential Φ_0 on the particle. For dilute solutions, the activity of the solution approaches 1 and eq. (1.36) is reduced to the Nernst equation

$$\Phi_0 = -\frac{k_B T}{z_i F} \ln a_i^{surf} = -\frac{k_B T}{z_i F} \ln a \tag{1.36a}$$

In addition, activity can be replaced by concentration for dilute solutions.

When the ions are adsorbed from the solution in amounts equivalent to the surface charge, the electrical potential of the particle surface is zero. These zero surface potential concentrations can be calculated from the Nernst equation by setting $\Phi_0 = 0$. The particle

grows in size under the condition of zero surface potential. At other concentrations, the particle acquires a positive or a negative potential according to the ion that is preferentially adsorbed on the particle surface. For colloidal particles that have weak acidic or basic groups, H^+ and OH^- ions are potential determining. In such a case, pH of the suspension medium is taken into consideration, instead of the ion concentration as in the case of ionic particles. At the pH corresponding to zero surface charge (isoelectric point), repulsive forces no longer exist and attractive forces dominate the interactions between the particles.

Charge reversing ions are selectively adsorbed from the suspension medium which changes the composition of the surface as well as the potential and the charge. Examples are the cationic surfactants adsorbed on clay (montmorillonite) particles and polyelectrolytes adsorbed on nanosized particles to maintain stabilization.

1.2.3 The DLVO theory

Charged particles are so abundant in nature and in industrial operations that their interactions were the first to be investigated historically. As initially formulated by the authors (Derjaguin and Landau, 1941; Verwey and Overbeek, 1948), the theory accepts the total interaction energy between two charged particles to be the sum of the repulsive and attractive forces:

$$U_T(h) = U_{att}(h) + U_{rep}(h) \tag{1.37}$$

The assumptions behind this statement are:

1. Particles have smooth surfaces with a uniform charge distribution.
2. Electrical double layer does not affect the van der Waals forces and these two forces are additive.
3. The charge density and the electrical potential of the surface are constant.
4. Uniform charge distribution is assumed to prevail at the surface.
5. The solid particles do not affect the molecular structure of the liquid suspension medium even at very close distances to the interface.

The attractive interaction potential is given by eq. (1.20a) for plate-like, flaky particles and by eqs. (1.25a) and (1.26a) for spherical particles. The repulsion term in eq. (1.37) inherently includes the molecular repulsion term of the Lennard–Jones potential given as the second term in the RHS of eq. (1.15). But this repulsion varies inversely with the 12th power of the distance between molecules and the range of effectiveness is too short to be significant in particle–particle interactions. As the particles approach each other under attractive forces in the suspension medium, another force of entropic origin evolves that keeps off the particles from approaching each other. The ionic distribution in the solution as two negatively charged particles approach each other is shown in Figure 1.2(b). As the particles approach each other, the diffuse double layer ions are confined in the space between the particles and the ionic concentration increases (Figure 1.2(c)). This confinement ends up with the evolution of a repulsion force due to the decrease in entropy in the interparticle space

that opposes further approach of the particles. If an electrolyte is present in the medium, the compressed diffuse layer will be in equilibrium with the bulk solution. In this case, the net pressure pushing the particles apart can be taken as the osmotic pressure between the compressed double layers and the suspension medium. Gouy–Chapmann solution permits linearization of the Poisson–Boltzmann equation, yielding the interaction energy *between flat plates* due to osmotic pressure as (Stokes and Evans, 1997)

$$U_{\text{rep}}(h) = 64C_{i\text{N}}^{0}\, k_B T \Gamma_0^2 \frac{\exp(-\kappa h)}{\kappa} \tag{1.38}$$

A similar expression can be obtained *for two spherical particles* of radius R, with the Derjaguin approximation

$$U_{\text{rep}}(h) = 64\pi R C_{i\text{N}}^{0} k_{\text{B}} T \Gamma_0^2 \frac{\exp(-\kappa h)}{\kappa^2} \tag{1.39}$$

With this expression, DLVO interaction energy given by eq. (1.37) *for two spherical particles* becomes

$$U_{\text{T}}(h) = -\frac{H_{121} R}{12h} + 64\pi R C_{iN}^{0} k_{\text{B}} T \Gamma_0^2 \frac{\exp(-\kappa h)}{\kappa^2} \tag{1.40}$$

This equation states that as the distance h between the particles increases, both the attractive and the repulsive terms tend to zero. If attractive forces dominate in the system, the total potential becomes negative, and if this domination is for a limited h range only, it results in a minimum in the total energy curve. If the repulsive forces dominate, the total potential becomes positive, resulting in a peak (repulsive energy barrier) if this domination is for a limited range in h, only. The shape of the attractive U_{att} and repulsive U_{rep} potentials are given in Figure 1.3(a), and the general shape of the total interaction potential in Figure 1.3(b). Core repulsion energy U_{CR} evolving from the overlap of the electron clouds is too short ranged to affect the total energy U_{T}, which determines the interactions between the particles. Figure 1.3(c) represents a case with an easily surmountable energy barrier U_{max} coupled by a deep potential energy minimum, the primary energy minimum (PM). Under such a case, the reaction or aggregation rate is controlled by the resistance of the suspension medium toward the motion of the particles only. Figure 1.3(d) represents a case of selectivity, where only the molecules with energies high enough to surmount the potential energy barrier (PEB) can aggregate. In Figure 1.3(e), a secondary minimum (SM) in the total energy profile is observed at distances of approach greater than the energy barrier. This means that there is no resistance to bonds formed in the range of the secondary minimum; but the reverse is also true: There is no resistance to the breakage of the bonds also. Reversible attachments as in the case of flocculation are formed in the range of the secondary minimum. Figure 1.3(f) is a case where there is no secondary minimum, but neither the energy minimum PM is very deep, nor the energy barrier U_{max}, very high. This allows the molecules with high enough energies to wander around for a better place to bond on the particle, called *restructuring*, as will be discussed in the next section.

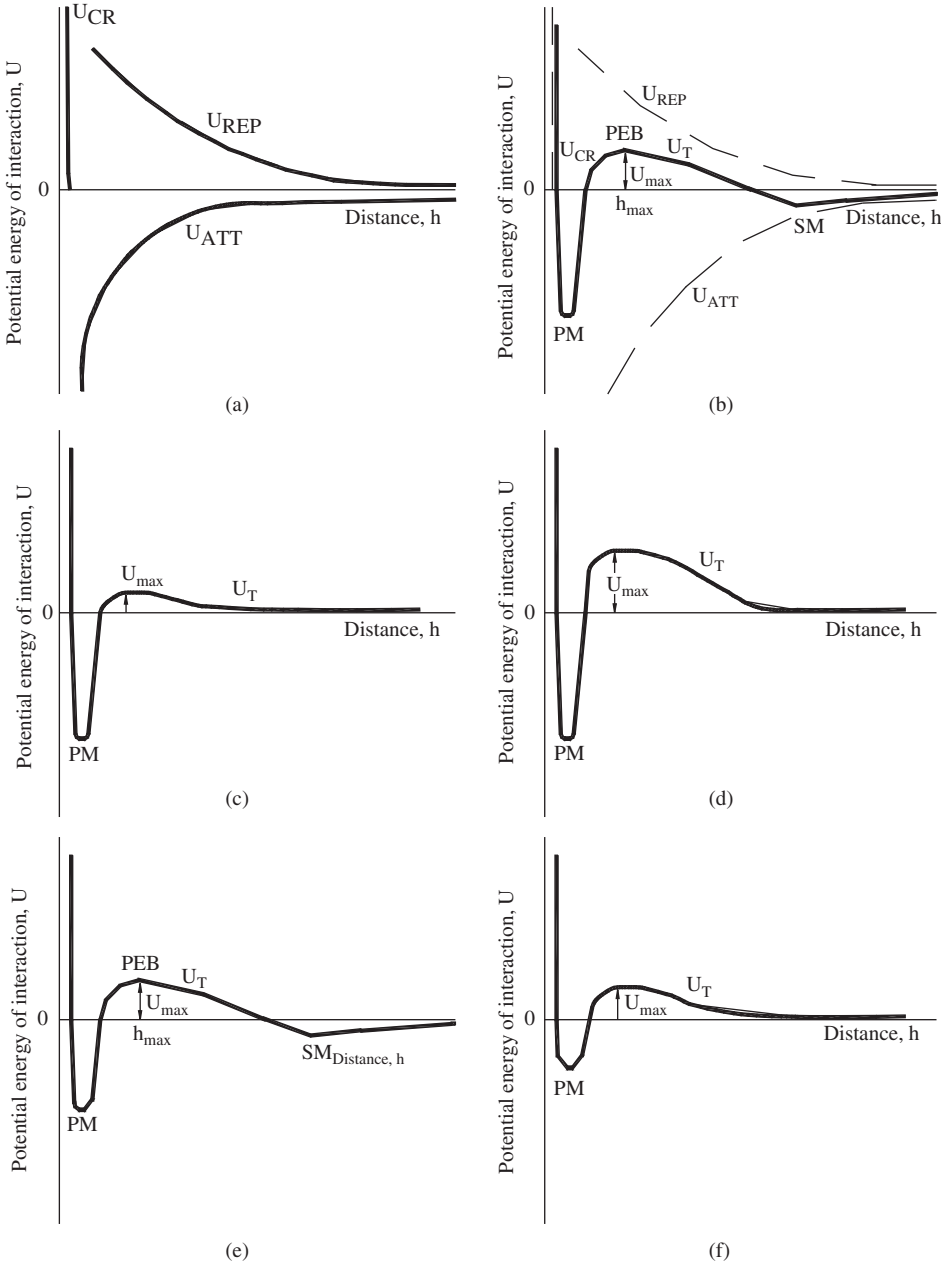

Figure 1.3 Variations in the potential energy of interaction with distance *h* from the surface of the particle. (a) Variation of potential energy under attractive and repulsive forces, (b) total potential energy of interaction, (c) total potential energy under low repulsive, high attractive forces, (d) case of a high repulsive energy barrier, (e) appearance of a secondary energy minimum and (f) low attractive and repulsive potential energies.

In any system of particles suspended in an electrolytic solution, the attractive and repulsive forces can be manipulated to maintain stabilization of the suspension, or to aid coagulation to bring about settling of the solid particles. The shape of the total interaction energy function determines which process will take place according to the average distance h between the particles. This distance is determined by electrostatic and hydrodynamic forces, as well as by the shape of the particles. The last two factors will be discussed in the following sections in connection with cluster formation. Electrostatically, the distance between the particles can be controlled by the Debye length, which in turn is a function of temperature, dielectric constant of the suspension medium, valence of the ions of the electrolyte, and the ionic concentration through eq. (1.34). The attraction and repulsion potentials are related to the properties of the suspension medium, through the parameters of the Hamaker constant and Debye length, respectively. For a given system of particles and suspension medium, the total interaction potential can be adjusted toward a given aim through the manipulation of repulsion forces by the addition of salt, an electrolyte, or by changing the temperature. Solution properties also affect the charge density on the surface of the particle, σ_0, in accordance with eq. (1.32). This effect on the charge density of the particle is not taken into account, according to the third assumption of the DLVO theory.

The validity of the DLVO theory at low to moderate ionic strengths of electrolyte solutions, where the distances between surfaces are large in comparison with molecular dimensions, is established through extensive experimental work. Electrostatic forces are present in a wide range of colloidal systems under moderate conditions and DLVO theory can be successfully used to evaluate the interactions between the particles. The DLVO theory fails to explain the interactions under (1) high ionic strengths, (2) heteroaggregation, (3) discrete surface charges, (4) strong electrostatic interactions as in the case of multivalent counterions or low dielectric constant of the solvent, and (5) specific ion effects. As the theory is based on bulk phase physical properties such as density and permittivity, it cannot be used to predict interaction potentials at very close distances of approach of the particles where the intervening suspension medium can no longer be taken as a continuum. Under such cases, solvation forces determine the interactions between particles.

When other colloids such as polymers, nanoparticles, and surfactants are present in the suspension medium, different forces, collectively called the non-DLVO forces, control the particle interactions.

1.3 INTERACTION OF PARTICLES DUE TO NON-DLVO FORCES

As the particles approach each other within a few molecular diameters, the intervening fluid behaves as discrete particles that have different properties from the bulk. Under these conditions, non-DLVO forces mainly of *entropic* origin dominate at very small separations and may overcome the effect of the DLVO forces. Depending on the interactions between the solid surface and the components of the suspending medium, these forces can be *oscillatory*, attractive (*hydrophobic*), or repulsive (*hydration*). In all cases, they decay exponentially within a few nanometers, corresponding to several molecular diameters, from the surface and coincide with the effective long-range DLVO forces between the particles.

Other non-DLVO forces of entropic origin arise due to the effect of osmotic pressures in the presence of adsorbed short-chain molecules (*steric forces*) or nonadsorbing polymers (*depletion forces*). Another non-DLVO force that is effective over long ranges and of energetic origin is called the *bridging force*. Bridging forces cause aggregation through simultaneous adsorption of high molecular weight polymers to more than one particle. Another type of bridging force arises when polymers grafted (chemically bonded) on different particles attract each other.

1.3.1 Forces of entropic origin

The fifth assumption of the DLVO theory, that the liquid in which the particles are suspended is not affected by the particle surfaces is believed not to be valid based on measurements with surface force apparatus (SFA) and atomic force microscope (AFM). The potential between a pair of particles can be affected by the interactions among the molecules of the suspending liquid medium; and between the liquid molecules and the molecules at the surfaces of the particles, called the *many-body interactions*. Especially if the solid surfaces are smooth and orderly structured, the liquid molecules in the immediate vicinity of the particles are affected also and form an ordered solvation layer, with properties significantly different from the bulk physical properties due to increased level of compaction. *Solvation* (*structural*) forces arise in between two particles when the free energy associated with the configuration of the surrounding solvent molecules changes as the particles approach each other (Israelachvili, 1991).

From the first and second laws of thermodynamics, the change in the free energy of interaction dw can be related to the internal energy and entropy through the relation

$$dw = dU - T\,dS \tag{1.41}$$

The change in the free energy of interaction is brought about by the decrease in the volume of the intervening liquid between the two particles. The increase in the concentration of this intervening layer causes the evolution of osmotic pressure between this layer and the bulk liquid phase

$$dw = -P^{\text{osm}}\,d\upsilon \tag{1.42}$$

Equating these two expressions for the free energy of interaction, the osmotic pressure can be related to the variation of internal energy and entropy with the decreasing volume in between the two particles through

$$P^{\text{osm}} = -\frac{dU}{d\upsilon} + T\frac{dS}{d\upsilon} \tag{1.43}$$

If there are no interactions between the molecules or colloids suspended in the medium, the internal energy does not change as the particles approach each other, the first term on the RHS of eq. (1.43) becomes zero and the osmotic pressure is controlled solely by variations in entropy. Entropy is related to the number of configurations Ω, which is a

function of the quantum states of the intervening molecules through the relation (Kuhn and Försterling, 2000)

$$dS = k_B \ln \frac{\Omega + d\Omega}{\Omega} \cong N k_B \ln\left(1 + \frac{d\upsilon}{\upsilon}\right) \tag{1.44}$$

where N is the number of solute molecules (or colloidal entities other than the particles) in the suspension medium. Since $\ln(1 + dv / v) \approx dv / v$, the equation simplifies to

$$dS = N k_B \frac{d\upsilon}{\upsilon} \tag{1.45}$$

and the osmotic pressure can be related to the concentration C_i of colloidal entities through

$$P^{osm} = k_B T \frac{N}{\upsilon} = R_G T C_i \tag{1.46}$$

where R_G is the universal gas constant. The difference between the osmotic pressures in the intervening layer and the bulk liquid gives the repulsive (or attractive) pressures operating between the particles: Regular arrays of molecules lead to a crystal-like structure with a packing density greater than that in the bulk. The osmotic pressure in the confined volume in between the particles then becomes greater than the bulk osmotic pressure, resulting in a net repulsive force. When the packing density of the distorted layers are approximately equal to the bulk packing density, the osmotic pressures become equal and the interaction between the particles are controlled by other forces operative at those distances. On the other extreme, when the intervening layer between the particles is so short as not to allow in the molecules or colloids, the osmotic pressure in between the particles become zero and less than the bulk osmotic pressure leading to strong attractive forces.

If there are only solvent molecules in between the particles, eq. (1.46) reduces to the *contact value theorem*

$$P(h) = k_B T[\rho_s(h) - \rho_s(\infty)] \tag{1.47}$$

where ρ_s is the molar density [mol m^{-3}] of the liquid at the surface of the particles, which is a function of the distance between the particles, h, with $0 < h < \infty$. Contact value theorem gives the pressure that arises due to a density increase in between two approaching particles, provided there is no interaction between the components of the intervening liquid and the particle surfaces (Israelachvili, 1991). This theorem can be used to find the pressure between two charged particles when ρ_s is used for the ion concentration at the surfaces; to give solvation interactions when ρ_s is the surface concentration of solvent molecules or to give the steric and depletion interactions when ρ_s is the surface concentration of polymers. The significance of this general application is that as long as a variation in the configurations of molecules or colloids in the intervening liquid are involved in the interaction of particles, the underlying mechanism is basically entropic in origin, even though energetic variations may also be present.

1.3.1.1 Oscillatory forces

In the case of simple molecules separating hard-sphere particles, a solvation force was found to arise when the liquid density changes as the surfaces approach each other. If the surfaces of the particles are smooth and unyielding, and the molecules in the confined space spherical with free access to the bulk liquid phase, the solvation force is a decaying oscillatory function of distance (Israelachvili, 1991)

$$P(h) \approx -k_B T \rho_s(\infty) \cos\left(\frac{2\pi h}{\sigma}\right) \exp\left(\frac{-h}{\sigma}\right) \tag{1.48}$$

where σ is the diameter of a liquid molecule. With simple molecules without any electrostatic repulsion, oscillations are superimposed on the attractive van der Waals force curve; i.e., the attractive force curve oscillates with a decaying amplitude until it converges with the long range van der Waals forces. The intercept of the oscillating curve with the force axis at contact ($h = 0$) gives the *adhesion force*. Depending on the relative dominance of other attractive and repulsive forces, oscillations were found to coincide with the attractive, repulsive, or total energy curves. If the liquid molecules are not symmetric, or the particle surfaces are not smooth, then no oscillations were observed. Instead, the energy curves varied monotonically with distance of separation (Israelachvili, 1991).

Similar oscillating phenomena are observed when colloids with regular shapes such as nanoparticles (Wasan *et al.*, 2005), and spherical micelles (Adler *et al.*, 2000) are suspended in a liquid used as a suspension medium for larger microparticles. The total potential energy curve oscillates in this case, due to unavoidable alignment of the nanoparticles at distances that are multiples of the nanoparticle diameters as the microscale particles approach each other. The oscillations in the interaction forces are given schematically in Figure 1.4 to illustrate the role of entropy. The unyielding hard walls of the microparticle surfaces force the smaller particles into alignment, which becomes more regular as the possible number of columns that can be formed decrease. The decrease in entropy due to ordering of the particles creates a repulsive force proportional to the order in the alignment. Thus, the amplitude of oscillations increase as the number of columns that can be fitted into the confined space decreases. Oscillations always end-up with a negative value, a strong attraction, at $h = 0$ due to depletion forces.

The oscillations die out after a separation distance of about five diameters of depletant molecules or colloids. Thus, the oscillatory forces are short ranged in comparison with the van der Waals forces with a range of 5 nm, when only simple molecules with a diameter of few Angstroms are present in the suspending medium. When the depletant molecules are colloids with diameters of several nanometers, the oscillating forces are considered to be long ranged in comparison with van der Waals forces.

There are two other forces whose existence are proven by experimental measurements (Israelachvili, 1991), even though the origins are not clearly understood but thought to be of entropic origin: Repulsive *hydration* forces and attractive *hydrophobic* forces in an aqueous suspending medium.

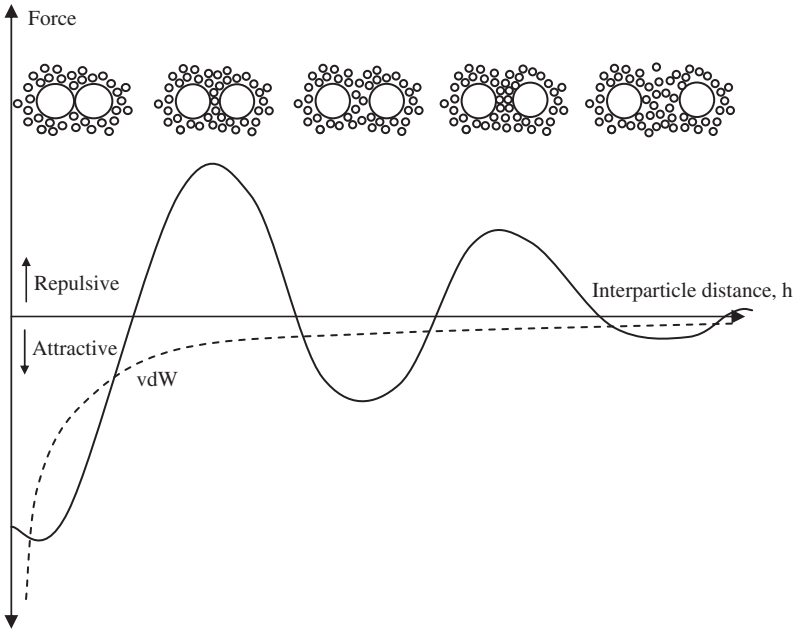

Figure 1.4 Oscillating forces.

1.3.1.2 Hydration forces

It is believed that, affected by the regular arrays of solid phase molecules, water molecules exist in a crystal structure adjacent to solid surfaces. The network extends a long distance away from the particle surface due to hydrogen bonds (type of van der Waals forces between H and O atoms in a molecule). If the hydrophilic surface of a particle forms stronger bonds with water, a strong repulsive force develops that decays exponentially within about 3–5 nm. Hydration forces can be controlled if the hydrophilicity of the surface can be regulated by ion exchange. If the hydrophilic groups are in-built within the surface structure of a particle, hydration forces exist under all conditions and stabilize the suspension.

1.3.1.3 Hydrophobic forces

Contrary to hydration forces, hydrophobic forces arise when the surface molecules of the particles have no attraction to water molecules, such as hydrocarbons and fluorocarbons and are responsible for the enclosure of the hydrocarbon groups within self-assemblies of surfactants. Hydrophobic forces are strongly attractive with a range and magnitude greater than the van der Waals forces. Recently, the attraction between two mica surfaces made hydrophobic with physisorbed double-chained cationic surfactant (dimethyl dioctadecyl ammonium bromide) was measured with the dynamic method in a SFA (Lin *et al.*, 2005). With this method, the distance–time variations of the surfaces could be detected down to separations of 10 Å. As the surfaces approached each other, the distance versus time paths first deviated from the trajectory based on viscous forces only and then converged to a single path

at the same points for all velocities of approach (10, 75, 115 Å sec^{-1}). The slope of this single path decreased at very short distances of approach (50 Å in the experiments) until the clarity was lost at the end (10 Å). The deceleration at very close distances was taken to be an indication of frictional losses within the liquid medium that persists even at such short separation distances. The convergence of the different paths was taken as an indication of a very strong short-range attraction that affects the stability. The authors concluded that what appears to be a hydrophobic force might be a combination of short-range and long-range forces as was suggested previously by other researchers. Reduced force curves as a function of distance are obtained by integration of experimental data taken as the variation of distance–time and are strongly dependent on the assumed boundary conditions which cannot be verified at the present. The reduced force curves calculated with the no slip assumption confirm the strong increase in force very near the surface ($h < 50$ Å), the origins of which are still unknown.

Polymers, short-chain hydrocarbon groups and nanoparticles also cause forces of entropic origin, repulsive *steric forces* and attractive *depletion forces*, as shown in Figure 1.5. They are analogous to attractive and repulsive counterparts of oscillating forces encountered at various distances of separation from the surface. The conditions in the colloidal system can be designed or engineered to enable these forces to be effective in stabilization or destabilization of suspensions.

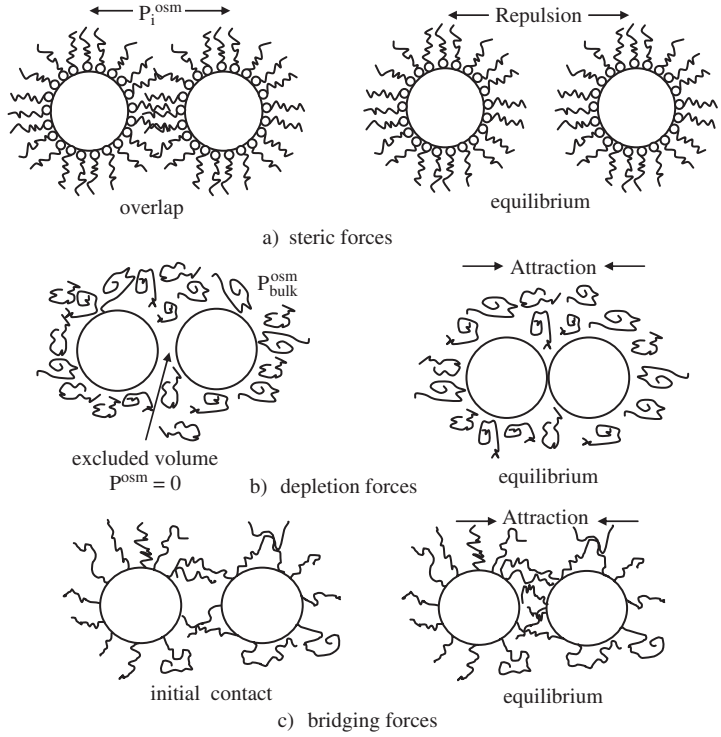

Figure 1.5 (a) Steric, (b) depletion, and (c) bridging forces at the initiation of the interaction and at equilibrium.

1.3.1.4 Depletion forces

Depletion forces arise when nonadsorbing polymers are present in the suspension medium. At a ratio of polymer to particle concentration depending on the properties and conditions of the system under consideration, the particles can approach each other up to such short distances that polymer molecules cannot enter the intervening layer. The osmotic pressure of the bulk liquid will then force the particles toward each other, as the P^{osm} will be zero in the confined intervening (excluded) volume (Figure 1.5(b)). The same effect can also be produced by nanoparticles, which do not adsorb on the surfaces of the micro- or macroscale particles but create an osmotic pressure outside of the confined layer sufficient to cause depletion forces to arise (Tohver *et al.*, 2001; Wasan *et al.*, 2005).

Basing on AFM measurements, Burns *et al.* (2002) found the depletion layer in polyacrylic acid (PAA) on polystyrene latex dispersion to decrease as the concentration of the polymer increased. The decrease was found to be very sharp at very low concentrations of the polymer, leveling off to a constant value of about 2 nm as the concentration increased. In very dilute polymer solutions, the thickness of the depletion layer increases as the molecular weight increases.

Fleer *et al.* (1984) relate the depletion force, F_{dep}, between a sphere and a flat plate to the depletion layer thickness Δ, through the area on which the osmotic pressure acts with the equation

$$F_{\text{dep}} = \pi P^{\text{osm}}(h + 2R_0)(h - 2\Delta) \tag{1.49}$$

where R_0 is the radius of the particles, h the interparticle separation, and Δ the depletion layer thickness. Accepting the depletion force to be additive to the attractive and repulsive forces of the DLVO theory, it is possible to observe a secondary minimum in the total energy curve, even when no such minimum exists in the presence of DLVO forces only.

1.3.1.5 Steric forces

Contrary to depletion forces, steric forces arise due to adsorbed molecules. These molecules could be surfactants, physically adsorbed polymers, grafted polymers that are chemisorbed at specific sites on the particle surface, freely dangling sections of polymers that are a part of the integral structure of the particle surface, or nanoparticles adsorbed on the particle surfaces. Repulsive forces arise when the adsorbed layers of the particles overlap on close approach, as sketched in Figure 1.5(a). Then, the increase in P_i^{osm} due to increased concentration in the overlap layer will cause the particles to repel each other. The closest distance of approach of the particles are determined by the chain length of surfactants, diameter of nanoparticles or radius of gyration R_{g} of the polymers given by

$$R_{\text{g}} = \frac{l(M/M_0)^{1/2}}{\sqrt{6}} \tag{1.50}$$

where M_0 is the molecular weight of the unit monomers with length l, M the molecular weight of the polymer made up of these monomers. Radius of gyration depends on the

compatibility of the polymer with the solvent. The polymer volume based on R_g includes the void spaces in between the coils and excluded volume within the polymer coils where solid segments cannot enter.

1.3.2 Forces of energetic origin

If the molecules or colloidal entities interact, then the internal energy term in eq. (1.43) should also be taken into account, where the internal energy, U

$$U = U_{el} + U_{trans} + U_{rot} + U_{vib} \tag{1.51}$$

is the sum of electronic, translational, rotational, and vibrational internal energies of the molecules, respectively. If the molecules attract each other, one or more of these internal energy components will change, causing the interaction to be *energetic* in origin, even though entropic considerations still play a role in the extension of the polymer chains. "*Bridging force*" is a term used to denote binding of particles within a network formed by simultaneous adsorption of polymers to more than one particle: If the solvent serving as the suspending medium for the particles is compatible with the polymer, the polymer stretches fully into the suspension medium. This is observed above a critical temperature called the *theta temperature*, T_θ, above which the liquid becomes an ideal solvent for the polymer. Polymers adsorbed on different particles may attract each other if there are segments available on the polymer chain that can react with each other. These segments can also adsorb on neighboring particles if there are available sites for adsorption on the particles. If the polymer length is long enough as in Figure 1.5(c), then the particles can be attracted to each other even though the net interactive DLVO force between the particles is repulsive.

Steric forces stabilize the particles in suspension. The microstructure of the aggregates formed by depletion forces is closely spaced particles. Bridging forces create highly porous clusters. The consequences of the microstructure of the aggregates on their rheological properties will be examined in Chapter 3, and on their sedimentation rate in Chapter 4. The surface forces responsible for interactions between particles and cases where such interactions are observed are summarized in Table 1.2.

1.4 AGGREGATION OF PARTICLES

Unless the particles are neutrally buoyant, that is they have the same density as the suspending medium, all particles will settle under the action of gravity. The smaller the particle diameter, the slower will be the settling rate as will be explicated in Chapter 4. In the case of colloidal particles, the settling rate may be extremely slow for the suspension to be kinetically stable, even though it is thermodynamically unstable. Kinetic stability is maintained if aggregation is prevented through repulsive forces. Destabilization begins when repulsive forces cannot counterbalance attractive forces.

Table 1.2

Summary of surface forces

Force	Effect[a]	Cause	Observed in
van der Waals	A	Asymmetric distribution of electrons	van der Waals forces are present in every case from the molecule to the particles and will tend to aggregate particles if not resisted by a repulsive force.
Double layer	R	Decrease in entropy due to overlap of diffuse ionic layers	Charged particles, microorganisms, uncharged particles that adsorb charged ions from the medium, ionic surfactant micelles, red blood cells
Oscillatory	A/R	Decrease in entropy due to alignment in the confined volume between approaching particles	Smooth, hard surfaced particles suspended in symmetric molecules or in nanofluids
Hydration	R	Entropic due to attractions between water and surface being greater than that among water molecules	Colloids with hydrophilic surfaces such as those bearing silicate, phosphate groups or polyalcohols: clays, silicates in ceramics, particles on which sugar based surfactants are adsorbed
Hydrophobic	A	Entropic due to incompatibility of surface molecules with water molecules	Folding of protein chains, self-assemblies of surfactants, nonwetting characteristics, separation of minerals by froth flotation
Depletion	A	Entropic due to excluded volume between particles	Red blood cell aggregation to form rouleaux, destabilization of colloidal particle suspensions at low polymer or nanoparticle concentration
Steric	R	Entropic due to increase in P^{osm} in regions of overlap	Stabilization of particle suspensions in all scales, pattern formation in nanoparticles, prevention of collapse in micelles and bilayers
Bridging	A	Energetic due to simultaneous adsorption of a polymer chain to more than one colloidal particle	Coagulation for separation of colloids in wastewater treatment plants. Aggregation of microorganisms

[a]R, repulsive; A, attractive.

1.4.1 Kinetics of aggregation

The crucial step in the destabilization of colloids is the formation of a dimer, as implicated within the context of surface forces given above. Once formed, these dimers aggregate through further collisions. After a nucleus is formed, the initial growth process proceeds by the addition of individual particles to the cluster. If the shear rate prevalent in the aggregation medium is not high enough to break apart the attachments formed, cluster–cluster unions may also take place.

The aggregation process involves two basic steps: The first step is the transportation of the particles to the aggregation site. Transportation can be brought about by random thermal Brownian motion (*perikinetic aggregation*), by the effect of a shear field inducing different velocities to the particles (*orthokinetic aggregation*), or through a difference in the terminal velocities in differential sedimentation. Transportation step ends with an inevitable collision between the particles. The frequency with which the particles collide with each other per unit time and unit volume is called the *collision frequency*. Collision frequency depends on the hydrodynamics of the medium, the volume occupied by the clusters (Birdi, 1993; Vicsek, 1999), and the average number concentration of particles within a cluster, which in turn depends on the level of shear stress the bonds within the clusters can withstand.

The second step is the formation of a bond between the two particles. The success of the collision in causing such a bond is rated as the *collision efficiency*, which depends on the shape of the interaction potential between the particles. A deep minimum in the potential with a negligible repulsive barrier, as in Figure 1.3(c) leads to *diffusion-limited aggregation* (DLA), whereas, an increase in the repulsive energy barrier (Figure 1.3(d)) causes reaction limited aggregation (RLA). In the limiting case of an insurmountable energy barrier, colloidal stability is maintained under the prevalent conditions.

The presence of a high repulsive barrier is not enough to prevent destabilization if there is a second minimum observed in the potential energy profile, as given in Figure 1.3(e). An energetically low second attractive minimum at distances larger than the repulsive barrier in the potential energy curve leads to reversibility in cluster formation: Aggregation and fragmentation processes occur simultaneously during growth, since the escape of a captured particle cannot be prevented if the depth of the minimum is not deep enough. If the captured particle is in the primary minimum that is not deep enough with a relatively surmountable energy barrier, as in Figure 1.3(f), then external forces applied can only bring about restructuring, ending up with the formation of more compact clusters.

The rate processes involved in aggregation can be given compactly by the expression

$$r = \alpha(i,j)\beta(i,j)n_i n_j \tag{1.52}$$

where r is the rate of aggregation in terms of number of particles $[m^{-3}t^{-1}]$, α the dimensionless collision efficiency factor, and β the collision frequency factor $[m^3t^{-1}]$, n_i and n_j the number concentrations of components i and j, respectively.

Aggregation rate based on a particle population balance was formulated for the first time by Smoluchowski (1917), and still used with some modifications and revisions today:

$$\frac{dn_k}{dt} = \frac{1}{2}\sum_{i+j=k} \beta(i,j) n_i n_j - \sum_{i=1}^{\infty} \beta(i,k)\, n_i n_k \tag{1.53}$$

The theory underlying population balances is given in Appendix B. This balance equation written for the conservation of particles of size k states that the rate of accumulation of particles of size k is equal to that formed by the collision of particles of size i and j (the first term on the RHS) minus the loss of particles of size k, due to enlargement through collision and aggregation with another particle of size i. This equation should be written for all sizes of particles within the range of high probability of occurrence. Smoluchowski made a number of assumptions to simplify the solutions of the resulting equations given in Appendix B. Collision efficiency α was taken as equal to one to eliminate the resistances due to adsorption and bond formation. This assumption presumes that all collisions end-up with bond formation. In later developments regarding the rate equations, the collision efficiency factor, α, is taken into account by the stability ratio W (Fuchs, 1934), defined as the inverse of collision efficiency factor α, or as the ratio of the rate constant of the fast diffusion limited aggregation (DLA) to the rate constant of the slow reaction limited aggregation (RLA)

$$W = \frac{k_{\text{fast}}}{k_{\text{slow}}} = \frac{1}{\alpha} \tag{1.54}$$

Stability ratio can also be defined in terms of potential energy of interaction, taking into account the effect of surface forces through the total energy potential, U_{T}

$$W = (R_i + R_j) \int_{r_i+r_j}^{\infty} \frac{\exp(-U_{\text{T}} / k_{\text{B}} T)}{s^2} ds \tag{1.55}$$

In this equation, R_i and R_j are the radii of the colliding particles, U_{T} the total energy including the repulsive and attractive forces, k_{B} the Boltzman constant, T the temperature, and s the distance between the centers of the particles.

U_{T} is generally calculated with the DLVO theory. If other forces are also effective, the necessary terms are added to the U_{T} expression if they can be identified. In actual practice, it is a hard task to integrate the effective forces, theoretical basis of which are not well developed yet.

1.4.2 Structure of aggregates

Aggregates range from highly porous structures with weak bonds in between the primary particles, called *flocculates*, to gel-like structures, called *coagulates*. *Cluster* is a more general term denoting aggregates of any size range, heterogeneity, and strength of interactive forces. Structure of clusters can range from extreme order as in a crystal to a completely amorphous mass. Clusters are formed by random collisions of particles in suspension.

Crystal structures can not form unless all the particles are homogeneous and strong attractive forces exist among them. On the other hand, completely amorphous clusters are formed by heterogeneous particles and polymers. The most frequently encountered structure in the aggregation of particles is a self-repeating pattern, called a *fractal,* which reflects the sequential stepwise formation mechanism of the cluster.

1.4.2.1 Fractal theory

Steric effects orient the collision of particles to such an extent that aggregation proceeds through preferable sites, resulting in a pattern formation. Sterically inhibited sites result in an increase in the porosity and in the variation in the distribution of porosity within the volume of the aggregate, so that its shape cannot be described by any of the geometrical forms. Fractal theory developed by Mandelbrot (1983) defines the volume, υ, of the particles with a noninteger power of the characteristic dimension, L

$$\upsilon \approx L^{d_f} \tag{1.56}$$

where d_f, the *fractal dimension*, is a nondigit number, a fraction, whence the name fractal originates. The fractal dimension d_f of a particle is always less than three, the dimension of the geometrical form enveloping the fractal object

$$\upsilon \propto L^3 \tag{1.57}$$

The relation between the mass, M, and the characteristic length, such as the average radius R_{agg} of a fractal aggregate, arises from the repeating forms of fractal aggregates. For a fractal object made up of N particles of mass m and radius R_0

$$N = \frac{M(R_{agg}, R_0)}{m(R_0)} = \frac{\rho_{agg} R^3_{agg}}{\rho_p R_0^3} \tag{1.58}$$

Clearly, the density of the aggregate is less than the density of the particle ($\rho_{agg} < \rho_p$) proportional to the porosity of the aggregate. To take into account the porous structure of the aggregates, the mass M can be expressed with the d_f power of R_{agg}, where $d_f<3$

$$N = \frac{M(R_{agg}, R_0)}{m(R_0)} \propto \frac{R_{agg}^{d_f}}{R_0^3} \tag{1.59}$$

If the same repeating structure prevails throughout the aggregate, then d_f becomes independent of the size of the cluster. This equation also describes the scale invariance or self-similarity of the fractal aggregates: The geometrical shape remains the same under isotropic rescaling of lengths (Meakin, 1998), such as that between two aggregates of mass M_2 and M_1 and radius R_2 and R_1

$$d_f = \frac{\log(M_2 / M_1)}{\log(R_2 / R_1)} \tag{1.60}$$

Clusters can grow by two types of mechanisms (Vicsek, 1999): In the first type of cluster formation, the structure of the whole cluster can affect the probability of addition to a site at a given position. Clusters formed under *diffusion-limited* (DLA) or *reaction-limited* (RLA) conditions, and clusters undergoing simultaneous aggregation–fragmentation processes (*restructuring*) during the growth process belong to this group. In these cases, fractal clusters are characterized by the radius of the cluster, fractal dimension and related with it, the density of the aggregates, as given by eqs. (1.56–1.58). In homogeneous fractal aggregates, an increase in the characteristic radius R at a ratio of λ, is reflected onto the mass of the aggregate as the d_f power of λ, λ^{d_f}

$$M(\lambda R) \approx C_1 \lambda^{d_f} (R)^{d_f} \tag{1.61}$$

Since the mass of the aggregate varies with a power of R that is less than the variation of its volume ($d_f < 3$), density of the aggregates decreases with an increase in their size. This decrease in density toward the edges of fractal clusters is exemplified in the case of $ZnCO_3$ nanoparticles forming a fractal aggregate (Ikizler, 2005) in Figure 1.6.

In the second type of cluster formation, the growth is local and depends only on the immediate environment of the position to which a new particle or cluster is to be added. *Percolation clusters* and *gels* belong to this group and may have a much greater porosity than the first type of clusters if growth proceeds along preferential sites. Self-similarity of the structure with an increase in the size is not valid in the case of gels described by percolation theory (Meakin, 1998; Berthon *et al.*, 2001; Takenaka *et al.*, 2004). These types of clusters are called *statistically self-similar fractals*, as the statistical quantities used in characterization remain invariant to a change in length scales, provided the length scale remains in the range between the characteristic length of the particles, r, and the cluster, R.

The composition of the medium between the particles affects the mechanism of cluster formation through its effect on the surface forces bringing about the interactions. In the previous sections, attractive forces were observed to have different ranges causing bonds of different strengths among particles. Fractal dimension represents the mechanisms effective in the aggregation process; namely, the effect of surface forces binding

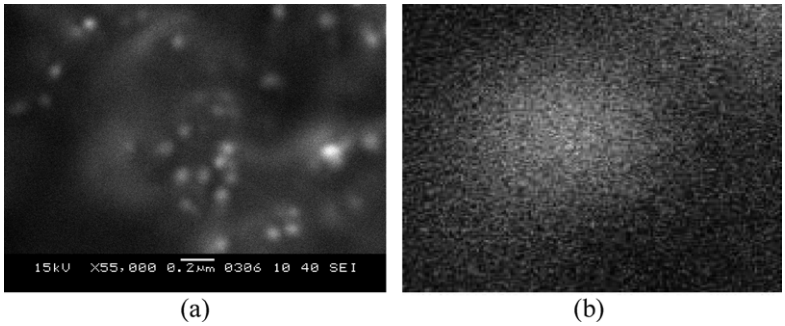

Figure 1.6 Fractal structure of $ZnCO_3$ nanoparticles (a) clusters and (b) detail of a cluster.

the components of the cluster and the hydrodynamics of the system, which may be effective in bringing together or tearing apart the components of the cluster. Under stagnant conditions where particles form the cluster through collisions resulting from random Brownian motion, the fractal dimension, d_f, represents the role of surface forces on the structure of resulting aggregates. When only DLVO forces are effective in the process, the magnitude of d_f gives an indication of the kinetics of aggregation during the formation, and the extent of fragmentation and restructuring in later stages. Non-DLVO forces operative in the aggregation process change the variation of the magnitude of d_f with the rate of aggregation from that expected under the action of DLVO forces alone.

1.4.2.2 Factors that affect the fractal dimension

Fractal dimension is affected by (a) the size and shape of component or primary particles, (b) the hydrodynamic forces that bring them to close approach, and (c) the surface forces that bind these particles. Only a brief review on these three basic factors will be given here. Actually all the factors that affect the surface forces also affect the aggregate structure and the fractal dimension. A more extensive review of these issues on the structure of fractal aggregates is given in Peker (2006).

1.4.2.2.1 Effect of the shape factor of primary particles on the fractal dimension

The primary particles making up the aggregates are generally assumed spherical for mathematical simplicity. Advent of nanotechnologies necessitates the stability of suspensions of hexagonal micelles, rod shaped nanoparticles and nanotubes, which cannot be handled with the assumption of spherical geometry. These dimensionally anisotropic particles are characterized by their length-to-diameter ratio, called the *aspect ratio*. Recently, Mohraz *et al.* (2004) studied the aggregation behavior of rod type boehmite colloids with aspect ratios, $\zeta = 3.9$, 8.6, and 30.1, and compared the results with the aspect ratio of spheres, $\zeta = 1$. Fractal dimension of the clusters formed under DLA conditions was found to be an increasing function of the monomer aspect ratio, with values of $d_f = 1.81$, 1.94, 2.14, and 2.21 for $\zeta = 1$, 3.9, 8.6, and 30.1, respectively. The simulated fractal dimensions varied in the range, $1.80 < d_f < 2.16$ for the aspect ratios $1 < \zeta < 11$, in good agreement with experimental results. In the aggregation of rod shaped particles, DLA and RLA regimes cannot be distinguished. As ζ increases, a more branched and compact structure is formed in comparison with the structure of the aggregates formed by spherical primary particles. Above an aspect ratio $\sim$8.6, d_f values of the aggregate structures were found to be approximately the same for both the DLA and RLA regimes. This was explained by the excluded volume effect of the rods that prevented them from penetrating into the pores of the aggregate structure, which were already compact due to the orientation of the rods.

Another work by Chen *et al.* (2004) on the aggregation behavior of nanotubes support the results obtained by Mohraz and coworkers (2004). Due to the flexibility and large aspect ratios of the nanotubes, entanglement becomes inevitable under the action of strong attractive dispersion forces. Determination of the fractal dimension by light scattering gave $d_f = 2.27$ for sterically stabilized and $d_f = 2.5$ for acid treated nanotubes.

1.4.2.2.2 Effect of fragmentation and restructuring on the fractal dimension

Shear stresses deform the aggregates, convective motion of the suspending medium causes the aggregates to extend, and stretch the bonds, collisions with other aggregates cause compression of the aggregates. These external forces cannot exert their full effect on the component particles, due to the fractal structure of the aggregates, i.e., the porosity and limited number of contacts per particle within the structure. The aggregate responds to the acting external forces by undergoing structural revision: If there is a weak bond in the structure, it may fracture and break apart, known as *fragmentation*. It may then recombine with the same or another aggregate under conditions that are more favorable. If the weak points can withstand the stress, then parts of the aggregate can rotate and form more bonds within it, called *restructuring*. In both cases, the aggregate becomes more compact reflected as an increase in the fractal dimension. Particles in the range of a few hundred nanometers undergo restructuring rather than fragmentation under low to moderate shear rates. In the process of restructuring, the diameter of the aggregate increases, passes through a maximum and then decreases, and levels off to an equilibrium size range. An increase in the diameter of the primary particles causes the equilibrium diameter of the aggregate to decrease.

The light scattering index (scattering exponent) SE in light scattering methods of particle size characterization is equivalent to fractal dimension d_f in compact structures and is used to characterize the degree of restructuring. In aggregates formed by small diameter particles in the order of a few hundred nanometers, SE is found by Selomulya *et al.* (2002) to approach the 2.6–3.0 range with time, much above the RLA limit of 2.1 for electrolyte induced aggregation. On the other hand, when the diameter of the primary particles approach the micrometer range, fragmentation–reaggregation process predominates over restructuring. The scattering index SE asymptotically approaches an equilibrium constant value in the range of 2.6–2.8 with time. The rate of approach to the equilibrium scattering index (SE) is directly proportional with the shear rate for all primary particle sizes.

1.4.2.2.3 Effect of DLVO forces on the fractal dimension

If the suspending medium of the colloids is a solution of indifferent electrolytes only, the colloids aggregate under the action of DLVO forces. The value of d_f is then determined only by the *mechanism* controlling the rate of aggregation. When *transport to the aggregation site is the only rate limiting factor* (DLA), the value of d_f was shown to vary in the range 1.7–1.8 by theoretical considerations (Jullien and Botet, 1987), and confirmed by experimental results of the aggregation of various colloids in solutions of different electrolytes (Lin *et al.*, 1990). When *adhesion to the cluster is the rate limiting step* (RLA), d_f was found to be in the range of 2.1–2.2 through simulations and experiments with electrolytes indifferent to the surfaces of the particles. These values are taken as criteria for testing the effect of a variable on the structure of the aggregates formed.

The rate of aggregation proceeding slowly due to PEBs (Figure 1.3) or steric hindrance is related to the rate of diffusion controlled aggregation through the stability ratio *W*. Aggregation may also proceed at an intermediate rate in between the two limiting cases of DLA and RLA,

representing zero and maximum PEBs for dimer formation, the initial step in aggregation. Berka and Rice (2005) obtained the relation

$$d_f = 0.17(\log W) + 1.67 \tag{1.62}$$

in the range, $5 < W < 100$, with dilute suspensions of natural kaolinite of particle size $R_h \approx 100 \pm 5$ nm through light scattering experiments. The limiting values of d_f estimated with this equation (eq. (1.62)) are 1.78 and 2.1, in agreement with the universally accepted values for the DLA and RLA regimes, respectively. Similar results were found for salt-induced aggregation of polystyrene particles (Tirado-Miranda, 2003). Fractal dimension varied linearly from 1.75 to 2.1 with an increase in the electrolyte concentration. In the more concentrated suspensions employed in industrial applications the compaction of the clusters and hence, the fractal dimension, may change during aggregation.

1.4.3 Role of polymers and polyelectrolytes on the coagulation of suspensions

Polymers and polyelectrolytes present in a suspension of solid particles, as in the case of paints, surface coatings, ceramics, wastewater suspensions, slow-release vehicles, bioreactors, blood, etc., have such a wide range of application that they deserve special attention. The effect of polymers on colloidal stability depends on the bonds formed with the particles, as well as on the chemical or electrolytic nature of the polymer. So a classification in terms of nonadsorbed and adsorbed polymers, and in the case of the latter, neutral or polyelectrolyte type of polymers would be more appropriate in terms of their effect on colloid stability. This classification should be preferred over grouping in terms of surface forces, since several forces can be simultaneously effective in particle–polymer interactions. Forces induced by the interactions of polymers present in the suspension such as *depletion*, *steric*, and *bridging* forces come to be effective in the aggregation of particles, *in addition to the DLVO forces* with a change in the pH, and ionic strength of the medium.

1.4.3.1 Particle–polyelectrolyte interactions

As most solid particles have charged surfaces, the interactions become more complicated when the polymer is a polyelectrolyte. In fact, polymer–particle interactions can be considered as a subgroup of polyelectrolyte–particle interactions at the *isoelectric point* of the polyelectrolyte when it is completely neutral. Recently, Claesson *et al*. (2005) reviewed polyelectrolyte–solid particle interactions under four categories.

1.4.3.1.1 Category 1: Polyelectrolytes adsorbed on oppositely charged particle

In this group of interactions, the charge density of both the polyelectrolyte and the particles affect the interaction as well as the pH and ionic strength of the medium. When polyelectrolytes and particles carry opposite charges, simple electrolytes such as Na^+Cl^- become competitive in adsorbing to vacant sites on the particle reducing the polyelectrolyte adsorption on the particles (*screening-reduced adsorption*). Repulsions between segments

of polyelectrolyte chains are affected by the screening also, ending up with large loops and extended polymer chains, increasing the thickness of the steric layer on the particles. On the other hand, if electrostatic forces are not negligible, screening reduces the repulsions between polyelectrolyte chain segments increasing the number of contact points with the particle surface, resulting in a thinner steric layer (*screening-enhanced adsorption*). Repulsion forces existing in the absence of polyelectrolyte can be converted into attractions at low concentrations of polyelectrolyte and ionic strengths sufficient to extend the polymer chains. If the particle/polymer ratio is sufficient to bring different particles within the reach of adsorbed polyelectrolytes, particles may be bridged together within a flocculate. Higher polyelectrolyte concentrations decrease the repulsive forces between particles through neutralization of their surface charge and may even cause charge reversal if adsorption is increased by nonelectrostatic attractions. Increase in the polymer charge density produces a thinner coating due to increased attachment sites along the chain; whereas, a decrease in the charge density of the polymer produces a thicker steric layer due to the size of loops in between the adsorption sites. On the other side, decrease in the charge density of the particle surface leads to adsorption of polyelectrolytes around the *discrete charges* increasing the *heterogeneity* of the particle surfaces.

1.4.3.1.2 Category 2: Polyelectrolytes adsorbed on uncharged particles

As adsorption decreases the entropy of the polyelectrolytes through restriction of random motion of polymer segments, adsorption is possible only if the enthalpy (energetic) variations are very favorable for adsorption to take place. Due to repulsion between chain segments, the polymers lie flat on the particle surfaces where the energetic effect is maximized. Presence of electrolytes in the medium screens the repulsive forces between polyelectrolyte segments, favoring the attractive forces between the particle and the polymer.

1.4.3.1.3 Category 3: Polyelectrolytes adsorbed on similarly charged particles

Polyelectrolytes adsorb on particles bearing the same charge only if the charge density is low and screened by the presence of simple electrolytes. If the charge densities of both the polyelectrolyte and the particle are high, then adsorption can be brought about by linkages with the cations of the second group in the periodic table. This linkage is strongly dependent on the hydration level of the cation: With the heavier cations in the group having low hydration levels, adsorption of charged polymer on the charged surface becomes quantitative leading to strong long-range repulsive forces and suspension stability. On the other hand, highly hydrated ions form limited number of bonds with the surface; but, as they also form bonds between polymer segments, bridging forces may lead to destabilization. These effects are optimized in the case of Ca^{2+} that can form bridges between similarly charged entities. The role of Ca^{2+} concentration is extremely important in such divergent cases as in coagulation and viscosity increase of blood and in determining the green (wet) and dry strengths of sand–clay mixtures in molds used for casting metals in the foundries. If the polyelectrolyte is not adsorbed on the particles and is linear, oscillatory forces can be observed that are of longer range and smaller amplitude in comparison with the oscillatory forces observed in pure liquids described above.

1.4.3.1.4 Category 4: Grafted polymers

Grafted polyelectrolytes are attached by chemisorption onto the particle surface; the type of interaction, steric or bridging, depends on the length of the polymer segments. This in turn is a function of the theta temperature, T_θ, in the case of neutral polymers and electrolyte concentrations in the case of charged polymer segments. In biological cells, segments of proteins extending out of the membrane as sensors also act as grafted polymers. Elasticity of the membrane of biological cells and microorganisms also has an effect on the interactions as explained in the next section.

1.4.3.2 Effect of polyelectrolyte interactions on the fractal dimension of clusters

There is only a limited number of experimental work done to determine the effect of parameters on the fractal dimension of the aggregate formed. Some of the results given in the literature are discussed here in terms of (1) nonadsorbing and (2) adsorbing polyelectrolytes to show their effect through depletion, bridging and steric forces.

1.4.3.2.1 Effect of nonadsorbing polyelectrolytes

AFM studies show that a secondary minimum in the potential energy profile of the particles may result because of the presence of nonadsorbing polymers (Milling, 1996, 1997; Burns *et al.*, 1999, 2002; Biggs *et al.*, 2000). The variation of the reduced force (force measured in an atomic force microscope (AFM) divided by the cantilever tip radius) with the distance of separation between the silicon-nitride cantilever tip and a flat silica surface is given by Burns *et al.* (2002) as a function of polyelectrolyte poly acrylic acid (PAA) concentration and molecular weight in Figure 1.7(a) and (b), respectively. The sections given in Figure 1.7(a) and (b) correspond to the secondary minimum after the PEB in Figure 1.3(e). The secondary minimum is caused by the summation of attractive depletion force and electrostatic repulsion force. In addition to the depletion forces, the increase in attractive forces is attributed to the reduction of electrical double layer repulsion in the presence of the charged polymers. At extremely low polyelectrolyte concentrations, depletion forces are negligible and the net force is repulsive without a secondary minimum. As the concentration of polymer increases, depletion forces also increase. The depth of the minimum increases and its position changes to lower separation distances. Increase in polyelectrolyte concentration produces a combined effect of reduction in double layer and depletion layer thicknesses. This effect is partially offset by a decrease in the depletion forces depending on the size and concentration of the polymer resulting in a leveling off of the total force at high concentrations as shown in Figure 1.8(a).

The depth of the secondary energy minimum given in Figure 1.7(a) in terms of force units is expressed as potential energy per unit surface area as a function of concentration of PAA in Figure 1.8(a), for the three molecular weights investigated by Burns *et al.* (2002). The negative sign of the ordinate indicates attractive energy. The secondary minimum approaches zero at extremely low concentrations of the polyelectrolyte. The energy of attraction decreases to lower negative values (the depth of the minimum increases in force units) as the concentration of polyelectrolyte increases, leveling off to a constant value at concentrations greater than $20\,\mathrm{g\,L^{-1}}$. Clearly, the depth of the attractive minimum

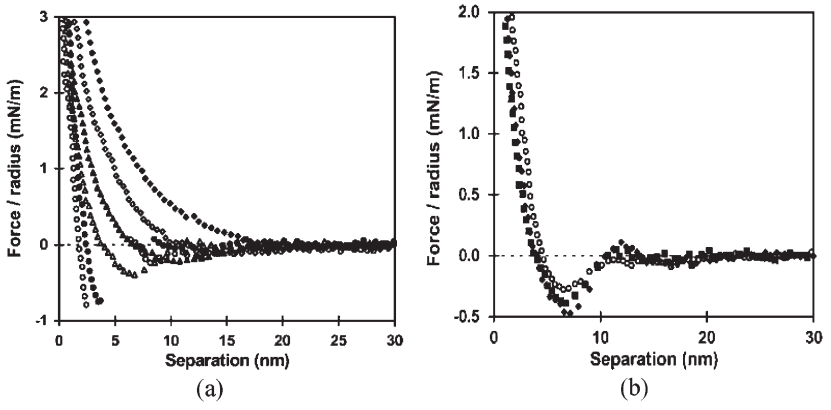

Figure 1.7 Reduced force (F/r_0) versus surface separation curves for a silicon nitride cantilever tip interacting with a flat silica surface: (a) in the presence of various concentrations of PAA (50,000 g mol^{-1}): (◆) 1 g L^{-1}, (◇) 3 g L^{-1}, (▲) 5 g L^{-1}, (△) 10 g L^{-1}, (●) 20 g L^{-1}, and (○) 40 g L^{-1} ; (b) in the presence of various PAA molecular weights: (◆) 250,000 g/mol, (■) 50,000 g mol^{-1}, and (○) 5000 g mol^{-1}, all at a fixed PAA concentration of 10 g L^{-1}. (Reproduced from Burns *et al*., 2002, with permission of Elsevier, Figures 6 and 7 in the original.)

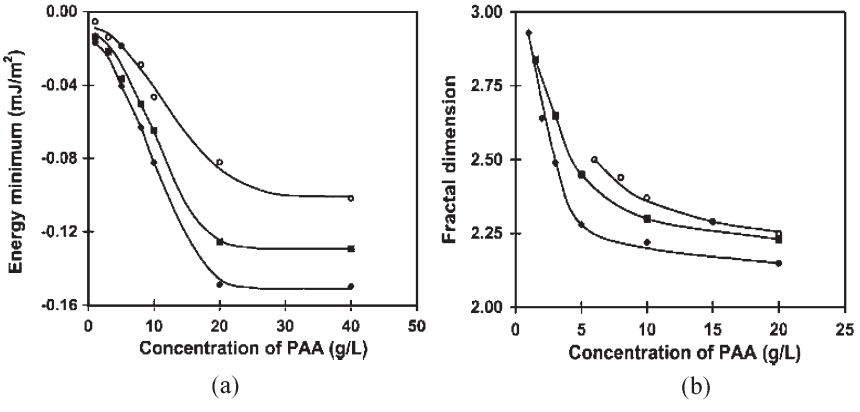

Figure 1.8 Dependence of the: (a) secondary energy minimum, (b) mass fractal dimension of aggregates of polystyrene latex particles, on changes in the PAA molecular weight and concentration (notation given in Figure 1.7(b)). (Reproduced from Burns *et al*., 2002, with permission of Elsevier, Figures 5 and 8 in the original.)

decreases as the molecular weight decreases. This shows that the bonds formed become reversible as molecular weight decreases. The shift of the minimum to smaller separation distances shows that more compact structures are to be expected as the concentration of polyelectrolyte increases.

The fractal dimensions of polystyrene latex particle aggregates in the presence of PAA in the same range of concentrations and molecular weights as in Figures 1.7(a) and 1.8(a) are given in Figure 1.8(b). The similarity in the shapes of the curves in Figures 1.8(a) and

(b) shows the effect of the depth of the secondary energy minimum on the structure of the aggregates. The low-energy of the secondary minimum allows the flocs to escape from their initial location and move around until they find an energetically more favorable place. The wandering of the detached flocs was physically observed by the authors under the microscope (Burns *et al.*, 1999). A high-energy minimum located at a short distance from the surface of the particle, observed at high polymer concentrations causes the aggregation to proceed in the RLA regime. The scattering exponent (SE) equivalent to the fractal dimension d_f, determined by static light scattering method, confirmed this physical model: At very high concentrations of the polymer, SE was found in the range of 2.0–2.2, inversely proportional with the particle concentration. At polymer concentrations less than $5\,g\,L^{-1}$, SE sharply increased with decreasing polymer concentration reaching a limit of 2.99 at $1\,g\,L^{-1}$ confirming the extensive restructuring that had taken place.

1.4.3.2.2 Effect of adsorbed polyelectrolytes

Effect of the presence of polymers on the structure formed by DLVO forces alone were observed by partially coating polysyrene particles with bovine serum albumin (BSA) molecules (Tirado-Miranda, et al., 2003). An overall increase in d_f of 0.3 units was observed irrespective of the pH, even though the configuration of the BSA molecules changed in the range investigated. At pH 4.8, the isoelectric point, the polyelectrolyte is at its most compact configuration. At pH 9, both the polystyrene particles and the polyelectrolyte are negatively charged. Polyelectrolyte coated particles were stable at pH 9 but aggregated with a close-packed structure of $d_f \sim 2.2$ at pH 4.8. The observed instability at the isoelectric point was attributed to the partial shielding of the particle charges by the neutral polyelectrolyte at its isoelectric point, causing the particles to come as close as 3 nm, a distance comparable with the length of polymer segments which "*bridge*" them within a compact aggregate.

Effect of the *steric* forces was investigated by varying the configuration of grafted polystyrene chains on silica particles in cyclohexane by varying the temperature above and below the theta (θ) point (Huang and Berg, 2004). The fractal dimension d_f was found to be a function of both time and temperature: It increased from a value of 1.75 at the transition temperature, to its equilibrium value of 2.13 with time while this equilibrium value increased to 2.84 as the temperature was decreased toward the end of the transition interval. Transformation to a more compact structure with time was attributed to spontaneous restructuring due to reduced rate of aggregation as the cluster size increased.

1.5 AGGREGATION OF FERROMAGNETIC PARTICLES

Interest in the aggregation of particles with magnetic properties increased recently due to the possibility of controlling their rheological and physical properties by an external magnetic field. A suspension of ferromagnetic particles of about 10 nm in diameter sterically stabilized by long-chain surfactants, or through electrostatic repulsion of adsorbed ions, is called a *ferrofluid*. As in other colloidal systems, the ferromagnetic particles interact through surface forces, such as van der Waals, electrostatic repulsion and steric forces.

In addition, the particles of a ferrofluid interact through long-range anisotropic dipole–dipole potentials. At low particle concentrations where there are no interactions between the suspended particles, a ferrofluid system behaves like an ideal paramagnetic gas. In this case, the equilibrium magnetization of the ferrofluid system M_L is given by the equation (Wang *et al.*, 2002)

$$M_L = n\frac{m}{\mu_0}\left(\coth\left(\frac{mH}{k_B T}\right) - \frac{k_B T}{mH}\right) \tag{1.63}$$

where n is the number concentration of particles, m the magnetic moment of the particles, μ_0 the magnetic permeability of vacuum, H the magnetic field, and the term in parenthesis is the Langevin function, connoting the relative effects of thermal energy ($k_B T$) and magnetic energy (mH). The initial susceptibility of the medium toward the effect of a magnetic field, χ_i is given by

$$\chi_i = \left(\frac{\mu_0 \mu^2}{3} n\right)\frac{1}{k_B T} \tag{1.64}$$

Dipole moment of a ferromagnetic particle, μ, is given as the product of its volume υ_M based on its magnetic radius, r_M, and its magnetization at saturation, m_s:

$$\mu = \left(\left(\frac{4}{3}\right)\pi r_M^3\right) m_s = \upsilon_M m_s \tag{1.65}$$

The initial magnetic susceptibility is seen to be a function of the volume fraction of particles, $n\upsilon_M$, from eqs. (1.64) and (1.65)

$$\chi_i = \frac{\mu_0 \mu m_s}{3}(n\upsilon_M)\frac{1}{k_B T} \tag{1.66}$$

Eq. (1.66) predicts a linear increase of the initial susceptibility with the particle concentration. Deviation from linearity signifies interaction between the particles, depicted by the dipolar coupling constant λ

$$\lambda = \frac{m^2}{4\pi\mu_0 d_p^3 k_B T} \tag{1.67}$$

where d_p is the particle diameter. Interaction between the particles increases as λ increases, or equivalently formation of aggregates enhances the magnetization of ferrofluids at weak magnetic fields. The thermal energy term in eq. (1.67) signifies that the aggregates formed are subjected to thermal fluctuations and are flexible. Under an applied external magnetic field, the dipole moments tend to align in the direction of the applied field in proportion to the field strength. This causes a lengthening of the needle-like strings into flexible chains together with unavoidable entanglement that causes the viscosity to increase.

1.5.1 Effect of the direction of the magnetic field on the aggregate structure

The structures formed on application of an external magnetic field depend on the relative directions of the magnetic field and the plane of the film of ferrofluids. Formation of chains of needle-like aggregate structures is observed when the magnetic field acts parallel to the film of magnetic particles. An increase in the field strength or in the concentration of particles causes more particles to aggregate, increasing the number and length of the chains. The spacing between the chains and the chain width decreases as the field strength H increases. When the magnetic field acts perpendicular to the ferrofluid film cylindrical magnetic columns are formed. The distance between the columns decreases as the field strength increases. The characteristic spacing in the ordered structures could be manipulated (Horng *et al.*, 2001) within a range from submicrometers to many micrometers by adjusting controlled parameters such as the magnetic field, the sweep rate, the film thickness, the concentration of the fluid and the temperature. Significant optical properties could be generated with these ordered structures.

1.5.2 Reversibility of aggregation

Reversibility of aggregate formation is an important issue if the end use of the ferrofluids is in the field of electronics. Ferromagnetic particles aggregate to reduce their enthalpy; but alignment in the form of strings decreases their entropy, so that aggregation and disintegration should be in balance dictated by the equilibrium conditions of the system. Klokkenburg and Erné (2006) tested the reversibility of zero-field aggregation of magnetic nanoparticles in a ferrofluid by two methods: By decreasing the dipole moments of the particles and by decreasing their concentration. Unoxidized iron–carbon particles ($Fe_{0.75}C_{0.25}$) in decalin stabilized sterically by polyisobutene were used in the first case. The particles were subjected to gradual oxidation to decrease their magnetic moments. Oxidation turned out to cause chemical interactions between the particles making the aggregation irreversible. Effect of a concentration decrease was tested on colloidal magnetite dispersions stabilized by surfactants. The results showed that zero-field dipolar structures disintegrated upon dilution indicating the reversibility of aggregation process through dipolar attractions.

Small-angle neutron scattering and light scattering measurements were used by Shen *et al.* (2001) to elucidate the structure of magnetite aggregates in aqueous and organic solvents stabilized by surfactants in *situ*. The magnetite particles were stabilized by a monolayer of adsorbed decanoic acid in organic (hexane) solvents. A second adsorptive coating by dodecanoic acid that would form a bilayer with the already adsorbed decanoic acid was necessary to reduce the attractive forces among hydrophobic surfaces in aqueous solutions and maintain stability through repulsion of the charged head groups. The results of the measurements indicated the formation of fractal structures with $d_f = 2.52$ and a characteristic dimension of 350 Å in aqueous media. As long as the second (outer) surfactant layer of the bilayer stabilizing the clusters could be kept intact, the cluster size remained stable. This was attributed to the increasing height of the PEB formed by the charged hydrophilic groups of the surfactants as the size of the cluster increased, approaching the $15k_BT$ limit for

electrostatic stability (Vold and Vold, 1983). The stability of these clusters in aqueous media was strongly dependent on the ionic strength of the medium, as stability is maintained by electrostatic forces only. In organic solvents where there is no electrostatic repulsion, small chain-like clusters with $d_f = 1.22$ and a characteristic dimension of 400 Å were formed, which were sensitive to volume fraction of the clusters in solution. Because of the orientation of the surfactant molecules of the coating in organic media, the surfactant layer does not make any contributions to the Hamaker constants because of the similarity of surfactant chains and the solvent molecules. In the absence of repulsive forces and weak van der Waals forces, the magnetite particles are expected to form chain-like structures by coupling end-to-end through the action of magnetic dipole moments. This is only a weak bond, however, because the magnetic dipole–dipole interactions are counteracted by the steric effect of the surfactant layer as well as the thermal energy, $k_B T$, resulting in the small size of the clusters, low d_f values and fragile chain-like structures that are sensitive to dilution.

1.5.3 Light-induced aggregation of ferrofluids

Recently, reversible light-induced aggregation in the absence of a magnetic field of ferromagnetic particles were reported (Hoffmann and Köhler, 2003; Kellner and Köhler, 2005). Magnetite particles of about 10 nm in size suspended in kerosene and initially stabilized by the steric action of an adsorbed layer of surfactants were found to aggregate when exposed to light. Light absorbance of the particles was maximum around 400 nm that decayed rapidly to a negligible constant value at wavelengths greater than 650 nm. The particles were found to aggregate to sizes reaching a few micrometers and moving randomly with Brownian motion when exposed to white tungsten light at an intensity of $100\,W\,m^{-2}$. The aggregates were found to disintegrate upon the use of a filter that permitted radiation greater than 645 nm. Two different rates of growth under reduced light intensities were attributed to fast initial aggregation of particles and a sequent slower growth of the clusters. The process was found to be completely reversible with no aging effects. When the same ferrofluid was subjected to a weak magnetic field, no aggregation was observed; but if light-induced aggregation was conducted under a weak magnetic field, isotropic clusters were formed as in the absence of a magnetic field, which then aligned along the magnetic field lines to form highly anisotropic linear superstructures. As a possible mechanism underlying the observed phenomenon of light-induced aggregation, an increase in the average population of the electronic states with higher electric polarizability than in the absence of light was proposed. The enhanced van der Waals forces could then overcome the steric barrier and cause the reversible aggregation.

1.6 FORMATION OF GLASSES AND GELS

Equilibrium states of solid particles are the crystal, liquid and gas states. Crystal states require close packed conditions satisfied through strong attractive forces between the particles at solid volume fractions of approximately, $\phi = 0.74$. When this close-packed structure is expanded in volume by about one-third, $\phi \approx 0.545$, rigidity of the hard sphere

crystal is lost (Poon, 2002 and the cited references). If the particles are still within the attractive potential field of each other, a dense liquid phase is observed. If the distance covered by the attractive potential field is less than the interparticle distance, a gas state is reached where the particles act independent of each other. A configuration different from the one expected at equilibrium for the same volume fraction of particles leads to nonequilibrium states of the suspension.

1.6.1 The glassy state

There are cases when crystallization is not observed even at $\phi \geq 0.58$. This is attributed to the local caging of particles, each particle being entrapped itself, besides being a member of a cage for surrounding particles (see Figure 3.1(e)). This nonequilibrium solid state is called, *glass*.

Pham *et al.* (2002) showed that two types of glass states could exist in a mixture of polymers and hard spheres at two different polymer to solid sphere ratios, corresponding to different modes of repulsive and attractive interactions. With a model system of sterically stabilized polymethylmethacrylate (PMMA) spheres ($R = 202\,\text{nm}$) suspended in decalin, which also contains nonadsorbing polystyrene ($R_g = 17\,\text{nm}$) they obtained the phase diagram given in Figure 1.9. When there is no polymer in the suspension fluid, fluid–crystal coexistence and crystal regions are observed as the volume fraction of PMMA particles

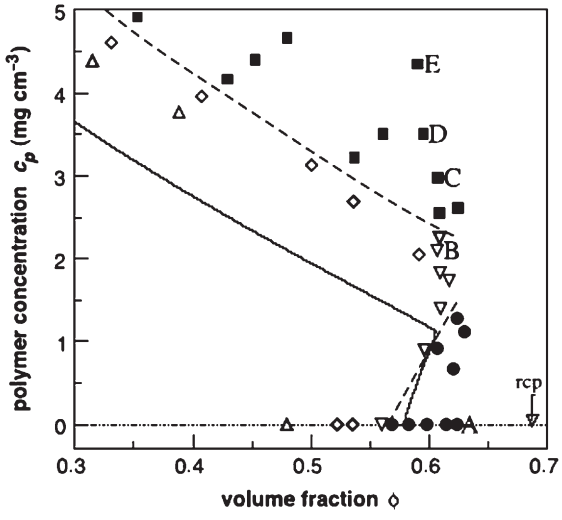

Figure 1.9 Equilibrium and nonequilibrium behavior of a colloid–polymer mixture at $R_g/R = 0.08$. Samples that reached thermal equilibrium (open symbols) are as follows: fluid (triangles), fluid–crystal coexistence (diamonds), and fully crystalline (inverted triangles). Samples that did not reach thermal equilibrium (solid symbols) are as follows: repulsion-driven glass (circles) and attraction-driven glasses (squares). Dashed curves are guides for the observed glass transition lines. Solid curves are Mode Coupling Theory predictions of glass transition lines. (Reproduced with the caption of Pham *et al.*, 2002, Figure 1 in the original with permission of Science AAAS.)

increased. Steric repulsion between the particles prevented crystal formation and glass state was observed above $\phi \geq 0.58$. As the polymer concentration was increased at constant solid particle fraction of $\phi \approx 0.6$, crystalline particles were observed again due to the action of depletion forces. Above the dashed line, denoting the glass transition lines, glassy states reentered the phase diagram, this time brought about by attractive forces. Glassy states are observed at high volume fractions of solid particles. This topic will be taken up again in relation to concentrated suspensions in Chapter 3.

1.6.2 Formation of gels

Another type of aggregation that confers non-Newtonian behavior to solid–liquid suspensions is gelation. A gel is a nonequilibrium state where the diffusive motions of the particles are prevented through long-range attractions. Recent studies show that even short-range forces in the order of a fraction of a particle radius can bring about gelation out of a homogeneous liquid phase if the attractive forces are strong, and concentrations high enough (Shah *et al.*, 2003 and the cited references). The requirement for gel formation is the existence of attractive forces between the particles sufficient to form a network spanning the available volume. The attractive forces can be anything such as bridging or electrostatic as in the case of clay (electrostatic), microemulsions (bridging of inverse micelles) and polymer suspensions (bridging) as given in Figure 1.10(a)–(c), respectively. In the case of particle–polymer mixtures where the polymers do not adsorb on the particles, depletion forces supply the required attraction. The stability of the suspensions depends on the strength of these attractive forces acting against thermal energy ($k_B T$) and hydrodynamic forces, as well as on the volume fraction of solids that maintain the stability of the network toward the action of gravity on the solid particles. The rheological properties are an indication of the stability of the gels, as will be explained in Chapter 2 for polymer gels and Chapter 3 for clay gels.

Gels are also formed by fractal aggregates. When the number and the size of the clusters are sufficient to fill the available space through edge-contact. Clusters formed by diffusion limited aggregation (DLA) are greatly ramified at the edges. Restructuring increases the compaction of the cluster indicated as an increase in d_f above that for reaction limited aggregation (RLA), simultaneously enlarging the void space between clusters opening up space for percolation of the suspending medium. If the cluster structure is very dense and particle concentration not sufficient to form a compact gel structure, clusters

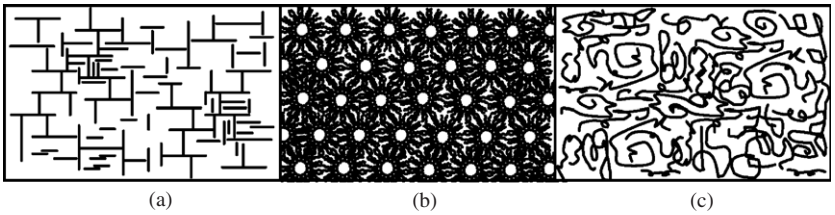

Figure 1.10 Various types of gels: (a) clay suspensions, (b) microemulsions, and (c) polymers in solution.

may settle under the action of gravity, as will be explained in Chapter 4. Very compact structures can also form in gels with a high volumetric fraction of particles (Shah *et al.*, 2003). The heterogeneity in the particle distribution necessitates the formation of voids, though they are very small as the attraction is controlled by depletion forces with the range of attraction proportional to the radius of gyration of the polymer, R_g, which is much less than the particle radius, R.

Fractal aggregates are also observed in gels of polymeric (Huang and Berg, 2004; Takenaka *et al.*, 2004) or microemulsion origin (Bordi *et al.*, 1996; Antalek *et al.*, 1997; Letamendia *et al.*, 1998), in fat-crystal networks (Narine and Marangoni, 1999) or in the sol–gel processes (Berthon *et al.*, 2001; Chiavacci *et al.*, 2004). Fractal dimension not only determines the compactness of the aggregate structure, but also affects the rheological behavior of concentrated suspensions (Lapasin *et al.*, 1998), and migration of charges resulting in an increase of the conductivity (Bordi *et al.*, 1996; Antalek *et al.*, 1997). Relaxation phenomena in critical microemulsion systems is attributed to the formation of transient polydispersed fractal aggregates of $d_f \sim 2.5$. Fractal dimension of ~ 2.5 was also obtained in different gel systems in experimental observations (Narine and Marangoni, 1999; Berthon *et al.*, 2001; Chiavacci *et al.*, 2004; Takenaka *et al.*, 2004).

Another type of gel of current interest is that formed by wormlike micelles, used as nanoreactors containing nanoclusters for the production of nanowires. Cylindrical micelles are made of surfactant molecules that pack-up in a liquid crystal structure. These cylindrical micelles align in a hexagonal order and continue growing length-wise until they span the available volume. Bouchama *et al.* (2004) investigated the thermal gel–fluid transitions of the hexagonal phase and showed that hexagonal phase can melt and recrystallize repeatedly, allowing trapping of various metal clusters in pre-prepared hexagonal phases.

1.7 SELF-ASSEMBLIES OF SURFACTANTS

In the previous sections, the polyelectrolyte molecules with electrophilic groups attached to a hydrocarbon chain were discussed in terms of the forces created by their local concentration and interactions with the particle surfaces. Surface active agents, or shortly surfactants, are similar to polyelectrolytes in that they are also amphiphilic molecules that have both a hydrophilic and a hydrophobic moiety in their structure. The main differences are that the hydrocarbon chains of the surfactants are much shorter than the backbone chain of the polyelectrolytes and they usually have only one or two hydrophilic groups gathered at one end of the molecule instead of being dispersed along the chain length. Surfactants have an immense area of applicability in processes related with emulsions, foams, as dispersion agents in suspensions, and in emerging technologies based on vesicles and microemulsions. The significance of surfactants in solid–liquid two phase flow resides on their use as stabilizing agents for microparticles, as flotation agents in mineral processing, as reactors for nanoparticles, as carriers in targeted delivery and slow release of drugs in the blood stream, as building blocks of the membranes of "soft" particles such as microorganisms and red blood cells (RBCs), and in drag reduction. Surfactants can be synthesized by conventional chemical synthesis or produced by living cells and microorganisms. Biologically produced surfactants generally have a much more complicated structure than the synthetically produced surfactants. Examples for the types of surfactants and their structures are given in Table 1.3.

Table 1.3

Types of surfactants and their structures

Type of surfactant	Example	Molecular structure
Anionic	Sodium dodecylbenzenesulphate	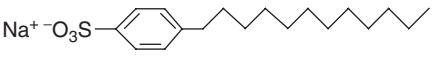
Cationic	Cetyltrimethylammonium bromide	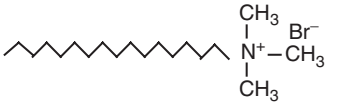
Nonionic	Polyoxyethylenesorbitan monooleate (Tween 80)	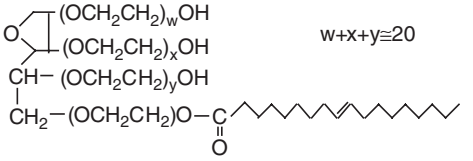
	Sorbitan monostearate (Span 60)	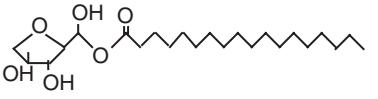
Zwitter ionic	Phosphatidyl ethanolamine	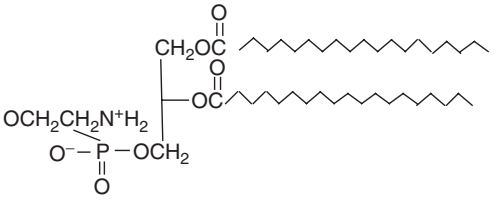
Double-chained	Sodium-bis(2-ethylhexyl)-sulfosuccinate (AOT)	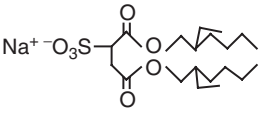
	Gemini surfactant	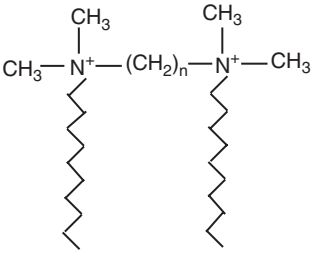

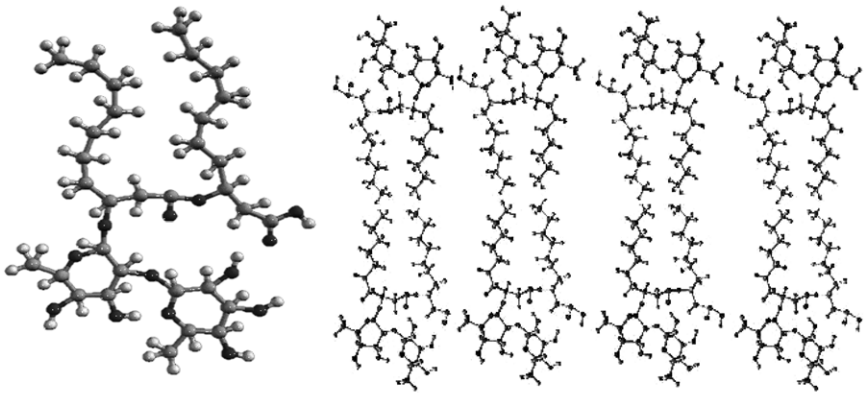

Figure 1.11 Rhamnolipid R2 surfactant, (a) in its minimum energy configuration and (b) in the form of bilayers.

To help in the visualization of the amphiphilic nature of a surfactant molecule and understanding of its orientation at interfaces, a render model of a biosurfactant, rhamnolipid R2, produced by *Pseudomonas aeruginosa* is given in Figure 1.11(a). The dark spheres denote oxygen, the small spheres, hydrogen, and large spheres, carbon atoms in the structure. The surfactant modeled at its minimum energy position with ChemSite Pro software has two decanoic acid groups coupled with an ester bond. A free carboxylic acid group is attached to one of the hydrocarbon chains and two rhamnose groups attached to the other chain. The two hydrocarbon chains are separated by the ester group. The lower part of the molecule including the carboxylic acid, rhamnose, and interconnecting ester group is rich in oxygen atoms and constitute the hydrophilic part of the molecule. The rest of hydrocarbon chains are rather short, with effectively eight methylene groups each, so the molecule preferentially dissolves in water. As the hydrophylic functional groups are connected by single bonds to the hydrocarbon chains they can reorientate depending on the interactions between the hydrophilic groups and the constituents of the aqueous medium (Peker *et al.*, 2003; Helvacı *et al.*, 2004; Özdemir *et al.*, 2004).

The presence of the hydrophobic groups within the structure of the surfactant molecule, makes its existence energetically unfavorable within the bulk medium, so the surfactant molecules are distributed in the form of *monomers* in solution, as *monolayers* at gas/liquid, liquid/liquid, or solid/liquid interfaces, whichever exists, or in the form of *micelles*. The total concentration of surfactants C_s^o in a system is the sum of all the concentration of surfactants in different states:

$$C_s^o = C_{mon} + C_{mly} + C_{mic} + C_{ads} \tag{1.68}$$

where C_{mon} is the monomer concentration, C_{mly} the concentration of surfactants that are associated as monolayers at gas/liquid interfaces, C_{ads} the concentration of surfactants adsorbed on solid surfaces and C_{mic} is the concentration in micellar aggregates. The solubility of the

monomers in aqueous solutions is determined by the relative volumes of the hydrophobic and hydrophilic groups in its structure, increasing with an increase in the latter. Surfactant molecules decrease their free energy by residing at interfaces, with the hydrophobic group oriented toward the nonpolar liquid in the case of two-liquid systems, toward air in the case of liquid–gas systems, toward the solid in the case of uncharged solid particles in an aqueous medium. C_{mly} is limited by the extent of gas/liquid interfacial area available in the macrosystem and the minimum area occupied by a surfactant molecule at the interface, a_{int}. C_{ads} is limited by the total surface area of the solids and the fraction of this area available for adsorption (*distribution of adsorption sites* or *fractional coverage*) depending on the heterogeneity of the solid surface. Finally, the remaining surfactants in solution will aggregate in the form of micelles.

1.7.1 Thermodynamics of self-assembly of surfactants

All forms of existence of surfactant molecules will be in equilibrium with each other including surfactants adsorbed on solid surfaces if adsorption is through reversible physical bonds only. Equilibrium condition, in the case of reversible aggregation, dictates that the free energy of a molecule (equivalent to its chemical potential) should be the same under all conditions. It is possible to find the concentration of each form of existence using the free energy relations. The number of surfactant molecules making up a micelle can be calculated starting with this principle. Adopting the notation of Israelachvili (1991), the chemical potential can be written as

$$\mu = \mu_N = \mu_N^0 + \frac{k_B T}{N} \ln \frac{X_N}{N} = \text{constant} \tag{1.69}$$

In this equation μ denotes the chemical potential, μ_N^0 is the mean interaction free energy per molecule or the standard free energy, N the number of surfactant molecules making up the aggregate and X is the concentration of the molecules in the aggregate in terms of mol fraction. As this relation is general it can be used to relate the free energy of the monomer with that of a molecule in the fully aggregated state:

$$\mu = \mu_N^0 + \frac{k_B T}{N} \ln \frac{X_N}{N} = \mu_1^0 + k_B T \ln X_1 \tag{1.70}$$

$$(\mu_1^0 - \mu_N^0) + k_B T \ln X_1 = \frac{k_B T}{N} \ln \frac{X_N}{N} \tag{1.71}$$

where the subscripts N and 1 indicate the aggregate and monomer, respectively.

The ratio of the concentrations in the associated and unassociated states is

$$\frac{(X_N / N)}{X_1^N} = \exp\left(-\frac{N(\mu_N^0 - \mu_1^0)}{k_B T} \right) \tag{1.72}$$

The term on the LHS of the equation is by definition, the equilibrium reaction constant K for the reversible formation and dissociation rates of the micelles

$$K = \frac{(X_N / N)}{X_1^N} = \frac{k_{\text{formation}}}{k_{\text{dissociation}}} \tag{1.73}$$

Micelles are dynamic aggregates with surfactant molecules going in and out of the micelle. The residence time of a surfactant molecule in the micelle, t_R, depends on the interactions of the molecule with the surrounding molecules in solution and in the aggregate, or equivalently the difference in the mean interaction free energies, $\mu_N^0 - \mu_1^0$. Characteristic collision time, t_0, of a molecule is then equal to the product of the mean residence time the molecule spends in the micelle and the probability that the energy of the collision will be sufficient for escape from the surrounding interacting molecules:

$$t_0 = t_R \exp\left(\frac{-\Delta E}{k_B T}\right) = t_R \exp\left(\frac{-(\mu_N^0 - \mu_1^0)}{k_B T}\right) \tag{1.74}$$

Characteristic collision time of surfactants is in the order of 10^{-9} sec for micelles and 10^{-7} sec for bilayers (Israelachvili, 1991). Therefore, the residence time of a surfactant in the micelle is a function of its interactions with the neighboring molecules. These interactions depend on the charge of the hydrophilic group, the van der Waals interactions between the hydrocarbon chains and between the O and H atoms in the hydrophilic group (H-bonds). As these interactions will be much stronger in double-chained surfactants with compact structures, their mean interaction free energies, μ_N^0 will be much lower than that of surfactants aggregated as spherical micelles, where the distance between hydrocarbon groups are increased due to curvature. Based on the characteristic collision time of surfactants, the membrane forming bilayers are expected to be much more stable than the spherical micelles.

1.7.2 Self-assemblies in solution

The concentration at which aggregation starts is called *critical micelle concentration* (CMC). This term is used exclusively for self-assembly of surfactants in solution. A more general term *critical aggregation concentration* (CAC), is also used for surfactant aggregation on solid surfaces, and aggregations in polymer–surfactant mixtures. The CMC depends on the *temperature*, *through the solubility;* and *structure* of surfactant molecules, *through steric effects*: Solubility of surfactants increase slightly with temperature up to a point called the *Krafft point*, after which it increases drastically. At concentrations below the solubility limit, the surfactant molecules exist in the form of monomers. The temperature should be above the Krafft point to prevent solubility becoming a parameter in the aggregation of surfactants. Micelles are formed at concentrations above the solubility and temperatures above the Krafft point of the surfactant. Various shapes of micelles are given in Figure 1.12. A model of bilayer formation by rhamnolipid R2 molecules is given in Figure 1.11(b). The shape that

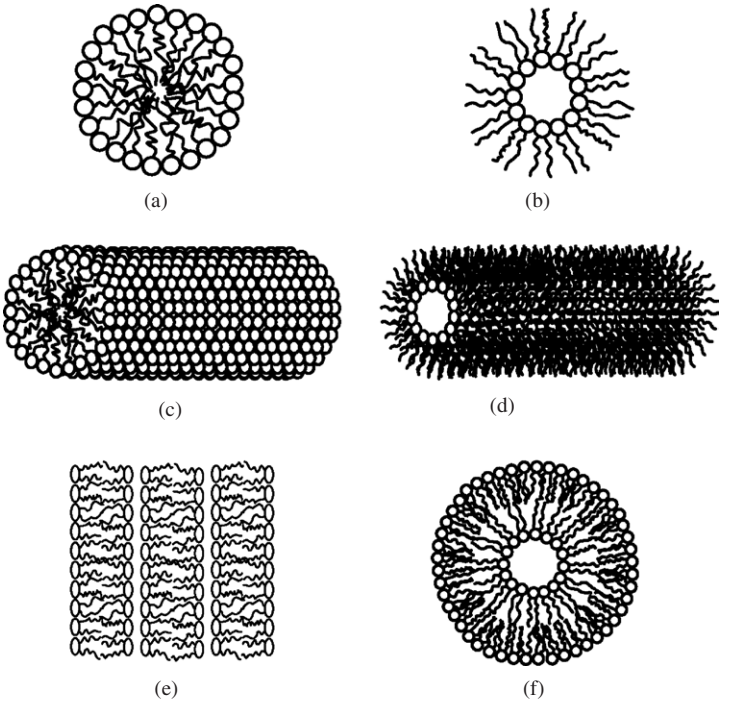

Figure 1.12 Types of micelles: (a) normal spherical, (b) reverse spherical, (c) normal hexagonal, (d) reverse hexagonal, (e) lamellar (bilayer) and (f) vesicle.

will be favored by a surfactant system depends on the type and structure of the surfactant, and the ionic strength of the solution, which will be discussed next.

The model of a rhamnolipid molecule, a double-chained surfactant at its minimum energy position given in Figure 1.11(a) could be circumscribed by a cylinder in three-dimensional space. Had there been only one hydrocarbon chain, the geometrical shape that would circumscribe the molecule would be a cone. The bulky hydrophilic head group would constitute the base and the hydrocarbon tail would determine the height of the cone. When a number of molecules would assemble, the preferred shape of the aggregate of single-chained surfactants would be a sphere and that of the double-chained, a flat layout, such as a bilayer, due to the inflexibility of the cylindrical form. In a bilayer, either the head groups, or the tails could be encompassed within the bilayer, depending on the continuous phase in between the double-layers. In the case of spherical micelles, the group that occupies the larger volume fraction constitutes the external surface. The compatibility of the external surface structure with that of the continuous medium determines in which phase the micelles exist: In the aqueous phase, the hydrophilic group constitutes the external phase, whereas in the oil phase, the hydrocarbon tails protrude out from the surface (inverse micelles). The in-between case would be a truncated cone, where cylindrical micelles would be favored, and orientation of the molecules being dependent on the external continuous phase. In geometrical terms, these conditions are expressed in terms of the

base area and height of the circumscribed volume of the molecule, known as the *critical packing parameter* (CPP):

$$\text{CPP} = \frac{\upsilon}{a_s l_c} \tag{1.75}$$

where υ is the volume of the molecule, a_s the area occupied by a molecule at an interface, and l_c the length of the hydrocarbon chain given in [Å] units by the equation

$$l_c = 1.54 + 1.265 n_C \tag{1.76}$$

where n_C is the number of carbon atoms in the hydrocarbon chain. A CPP value less than 1/3 signifies spherical micelles, 1/3<CPP<1/2, cylindrical micelles, 1/2<CPP<1, vesicles, and CPP≈1, bilayers.

The bilayer structure is of particular interest as it constitutes the cell membranes. Two properties of the bilayer are of particular importance, *elasticity*, and *bending modulus*. Balance between attractive and repulsive forces (in the case of ionic surfactants) determines the optimum interfacial area a_0 for a surfactant molecule, where the total interactive energy will be minimum. Just as in the case of spring forces, if the interfacial area is stretched, attractive forces will act to draw the molecules to the minimum area. In other words, the molecules at the interface behave elastically toward an extension or compression in the same plane. The elastic energy E_{el} [J], is given by

$$E_{el} = \frac{1}{2} K_{el} \left(\frac{(a - a_0)^2}{a} \right) \tag{1.77}$$

where a_0 is the optimum interfacial area, a the area under stretched conditions, and K_{el} the modulus of elasticity [Jm^{-2}]. Through energy considerations, modulus of elasticity is found to be $K_{el} \approx 2\gamma$ for monolayers and $K_{el} \approx 4\gamma$ for bilayers where γ is the surface tension (Israelachvili, 1991). Experimental values of the modulus of elasticity of fluid lipid bilayers and free biological cell membranes are found to be in the range of 0.10–0.23 $J\,m^{-2}$ (Kwok and Evans, 1981; Evans and Rawicz, 1990; Marsh, 1990).

Interaction between the hydrophilic and hydrophobic groups also leads to a resistance to bending or variation of radius of curvature of the bilayer (Israelachvili, 1991):

$$E_b = -2\gamma\delta \frac{d}{R^2} = \frac{1}{2} \frac{K_b}{R^2} \tag{1.78}$$

where E_b is the energy of bending [Jm^{-2}], δ the bilayer thickness, d the distance from the hydrocarbon–water interface where the repulsive forces are centered, R the radius of curvature, γ the surface tension [Jm^{-2}], and K_b the bending modulus [J]. When head-group repulsion dominates, d is positive and K_b is negative; and when chain repulsion dominates, d is negative and K_b is positive. Experimental values of K_b (positive) of fluid bilayers are in the range of $(2 - 20) \times 10^{-20}$J. When K_b is negative, stable vesicles cannot form, which occurs in the case of large repulsive head groups and short hydrocarbon chains.

Bilayers, biological membranes and other surfactant aggregates such as vesicles and micelles in microemulsions are not rigid but fluid-like, moving constantly under thermal fluctuations. In the case of bilayers and membranes, the component surfactant layers can move in wave-like motion (undulation), bringing about forces of entropic origin during these random motions (Israelachvili, 1991). The first of these, the *protrusion force* arises if a side chain dangling into the space between the component layers becomes "squeezed" during the random motion of the layers. The response is repulsion due to entropy decrease on confinement within a limited space. An *undulation force* arises during the wave-like motion of the membrane and is associated with the bending modulus K_b, as given above. The component surfactant layers of a membrane can also undergo peristaltic motion: The component layers may approach and retract from each other without bending. In this case, a *peristaltic force* arises related with the modulus of elasticity (or resistance to expansion) K_{el}. Resistance to close approach of the component layers also contributes to this force.

1.7.3 Self-assemblies on solid surfaces

Surfactants aggregate on the surfaces of solids on which they are adsorbed with the same motivation of reducing their free energy by secluding their hydrophobic groups from the aqueous phase. Surfactants may adsorb on surfaces either with their hydrophobic or with their hydrophilic groups. The first case occurs when the solid is hydrophobic. The hydrocarbon chain of the surfactant molecule is adsorbed on the solid surface, leaving the hydrophilic ends suspended in the aqueous solution. The net effect of this adsorption is similar to formation of micelles, with the particle enclosed by a layer of surfactants.

Since most solid surfaces are negatively charged, cationic surfactants are preferably adsorbed on the surfaces of the particle rendering it hydrophobic. This may be a desirable situation if the aim is suspension of the particles. Stabilization of the suspension occurs over a limited range of concentrations only, for the surfactants form a second layer (bilayer) on the free hydrocarbon chains with the hydrophilic groups facing the aqueous solution when present in concentrations in excess of that required for full coverage of the particle surfaces. Spherical or disc shaped micelle formation is also possible if the attractive forces between the hydrophobic chains are greater than the attractive forces between the solid surfaces and the hydrophilic groups. The CPP is an indication of the strength of adsorption of surfactants whether the solid surface is hydrophobic or hydrophilic: Adsorption increases as CPP increases (Jönsson *et al.*, 1998). Therefore, double-chained surfactants with CPP value ≈ 1 are preferably adsorbed on solid surfaces and are excellent suspension reagents. In the case of Gemini surfactants with double hydrocarbon chains and two cationic groups, both the increased adsorption energy of the two hydrophilic groups and density of the hydrocarbon chains contribute to the compactness of the adsorbed monolayer (Rabinovich *et al.*, 2005). A high repulsive barrier toward aggregation is formed even at the low CMC values of these surfactants. Addition of an electrolyte also increases the CPP leading to increased adsorption of ionic surfactants on solid surfaces. Maximum repulsive force was found to increase linearly with the chain length of the cationic surfactants (Adler *et al.*, 2000) at surfactant concentrations twice the CMC value. This maximum repulsion force that is an order of magnitude greater than expected from

electrostatic repulsion forces was attributed to elastic deformation of adsorbed surfactant layers and specifically to the resistance to compression of surfactant self-assemblies in the adsorbed layer, as will be explained below.

1.8 STABILIZATION OF SUSPENSIONS

In some processes, particularly technologies related with nanoparticles, stability of the suspension and control of the size distribution of the particles is a prerequisite for the expected performance of the particles. The only long-range repulsive forces that can be employed to overcome the attractions caused by ubiquitous van der Waals forces are double layer repulsions and steric forces. Double layer repulsions handled by the DLVO theory is relevant under mild strengths of electrolytes and pH. Stabilization by repulsive forces is used with success in operations involving particles in the micrometer scale. As the particle size is reduced to nanoranges, the charges carried by these small volume bodies decrease. The repulsive ionic cloud around these particles is not sufficient to overcome the attractive van der Waals forces, necessitating the employment of steric forces to maintain stabilization. Steric repulsion can be brought about by the adsorption of three different entities: (1) surfactants, (2) polymers and polyelectrolytes, (3) nanoparticles. As each of these methods is an issue of current interest and intensive research, some of the recent developments are summarized below.

1.8.1 Stabilization by surfactants

Stabilization by surfactants is a complicated phenomenon involving surfactant–surface, surfactant–surfactant, surfactant–solvent, and solvent–surface interactions. By manipulating these interactions, surface morphology, hydrophobicity, surface layer strength, and rheological properties can be changed according to the process requirements. In the flow of concentrated suspensions, in high shear processes such as mixing, and in extrusion of pastes, the adsorbed surfactant layers are forced to interact under high shear and close distances. To reduce the deformative and destructive effect of close approach under stress, the surfactant layer should have adequate yield strength and modulus of elasticity (Rabinovich *et al.*, 2004). In this section, structure of surfactant layers will be related to resistance toward deformation.

It is possible to change the surface morphology of solid particles by adsorption of surfactants. The surface concentration of surfactants Γ [mol m^{-2} or molecules $Å^{-2}$ units] on solid or liquid surfaces is in equilibrium with the bulk phase concentration or more correctly with the activity of surfactants in solution, determined by the Gibbs adsorption isotherm. Increase in the bulk concentration above that required for compact film formation at solid surfaces (Γ_{max}) changes the structure of the surfactant film on the solid surfaces. This concentration is closely related with the CMC or CAC of the surfactant. The structure of the film depends not only on the concentration but also on the structure of the surfactant and the hydrophobicity of the solid surface: Surfactants adsorb with their hydrocarbon chain on hydrophobic solid surfaces. As the bulk concentration increases, surface

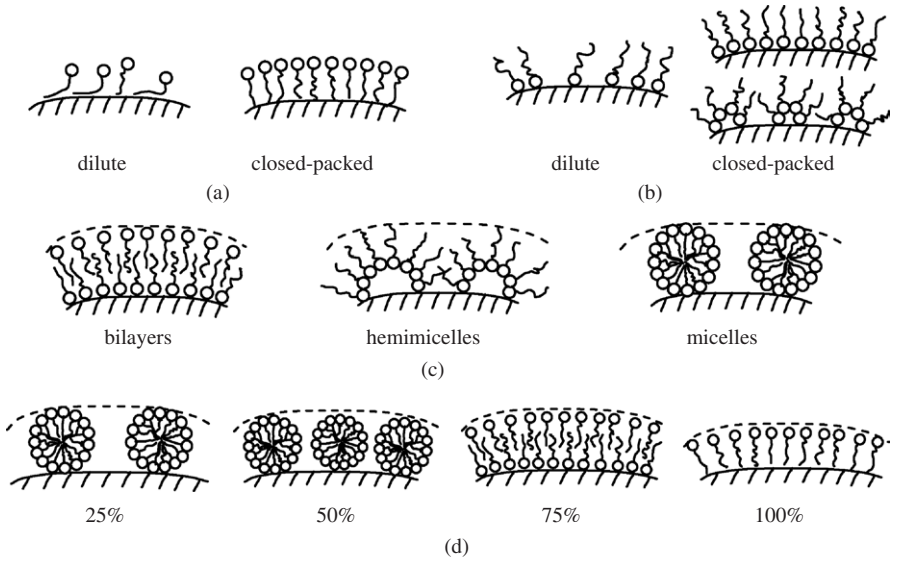

Figure 1.13 Structure of surfactant layers on solid surfaces. (a) Hydrophobic surfaces, (b) hydrophilic surfaces, (c) possible configurations at high surfactant concentrations and (d) variation of the layer structure with the hydrophobicity of the surface related with Figure 1.14.

concentration also increases, bringing the surfactant molecules into an upright position as depicted in Figure 1.13(a). At maximum concentration, only the hydrophilic groups are accessible from the exterior, rendering the particle hydrophilic. Surfactants adsorb with their hydrophilic groups on solids bearing an opposite charge, such as in the case of preferential adsorption of cationic surfactants on negatively charged clay surfaces. The structure of the surfactant film depends on the surface charge density of the solids. If uniform charge density prevails, as in the highly charged solids, then a similar compact monolayer forms rendering the solid surfaces hydrophobic, as in Figure 1.13(b). The surface morphology depends on the surfactant structure at higher concentrations. Possible configurations are shown in Figure 1.13(c).

1.8.1.1 Variation of surface forces with the structure of the surfactant layer

The structures in Figure 1.13(c) are for surfactants with head groups made up of electrophilic atoms only. Ethoxylate type of surfactants with hydrophilic end groups of the form [–O(–CH_2–CH_2–O)–H] are widely used in many processes and are of special interest. This group can attach to the surface by hydrogen bonds via –O– atoms, or through hydrophobic forces via the ethylene groups. Grant *et al.* (2000) prepared engineered surfaces by chemisorbing thiohexadecane ($CH_3(CH_2)_{15}$–SH) and thiohexadecanol ($CH_2OH(CH_2)_{15}$–SH) via –S– bridges on gold surfaces, so that the external surface of the particle would have known percentages of –CH_3 and –OH groups, thus, known percentage of hydrophobicity. They adsorbed an ethoxylate type of surfactant octa(oxyethylene) *n*-dodecyl ether ($C_{12}E_8$) on the engineered surface and measured the surface forces as a function of configuration of the

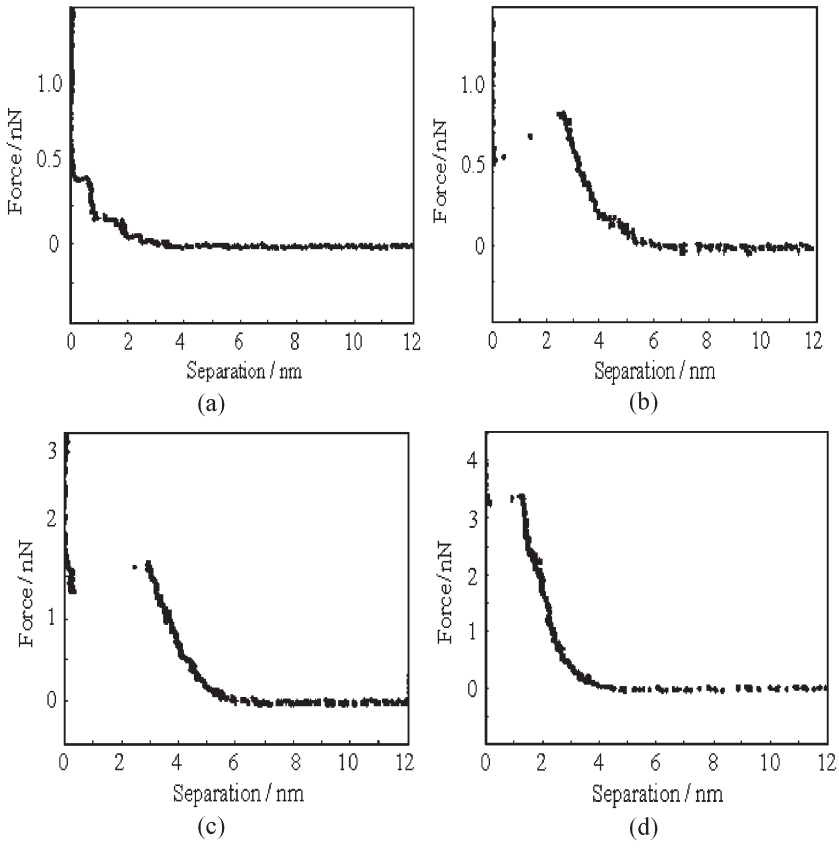

Figure 1.14 Forces between the AFM tip and the surface. (a) 25% CH_3 surface, (b) 50% CH_3 surface, (c) 75% CH_3 surface and (d) 100% CH_3 surface (Redrawn from Grant *et al.*, 2000. Figure 5 in the original, with permission of American Chemical Society).

surfactant layer. Possible surfactant layer structures in conformation with AFM images and force measurements are redrawn in Figure 1.13(d) and the variation of interactive forces with distance of approach are shown in Figure 1.14(a)–(d).

Figure 1.14(a) shows that there are no interactive forces between the AFM tip and the particle with a surface of 25% hydrophobicity up until a separation distance of ~2 nm. Resistive barrier is observed on further approach. The stepwise character of resistance implies that layers or groups with different adsorption strengths are being removed on approach of the tip, before the tip adheres with the surface, indicated by the steep rise in force at ~0 nm. The surface of adherence is the external surface of the thiohexane/hexadecanol layer that behaves as a solid surface because of the high strength of chemisorption. The continuity of the force curve indicates that the adsorbed ethoxylate layer is labile and escapes from the site of compression without being disrupted. The sharp rise of the repulsion barrier on approach of the tip and the break in the force curve indicates that the adsorbed ethoxylate layer structure is disrupted before the tip "jumps" into contact with the solid surface. As the hydrophobicity of

the surface increases, the height of the repulsion barrier before the disruption increases to higher values (Figure 1.14(b)). This shows the strength of adsorption, confirming that adsorption takes place through hydrophobic forces far outreaching the effect of van der Waals forces (hydrogen bonds) under the competition of water molecules of the suspension medium, which also try to adsorb to those hydrophilic –OH groups. The onset of the repulsive barrier indicates the layer thickness. The layer thicknesses at 50 and 75% hydrophobicity (Figure 1.14(b)–(c)) are similar (~6nm) almost twice the length of ethoxylate molecules. Either close-packed micelle formation or bilayer formation could have a layer thickness of this magnitude. Bilayer formation at 75% (Figure 1.14(c)) was inferred from the smooth appearance of the adsorbed layer (Grant *et al.*, 2000). The decrease in the onset value of resistance, together with an increase in the barrier height (force) indicates that a monolayer has formed with a concomitant reversal in the configuration of surfactant molecules, adsorbing much more strongly through the hydrocarbon chains than through the ethylene groups of the ethoxylate groups.

1.8.1.2 Deformability of surfactant coated particles

Work conducted on the resistance of adsorbed layers toward compression inferred from the force–distance profiles in AFM (Grant *et al.*, 2000; Adler *et al.*, 2000) show that surfactant chain length and configuration of the surfactants in the adsorbed layer has a strong bearing on the steric repulsion of the particles, sustaining the suspension stability. Steric repulsion acts through the yield stress and modulus of elasticity in terms of rheological properties (see Chapter 2). Rabinovich *et al.* (2004) analyzed the mechanical strength of the adsorbed layers through the Hertz (1986) theory taking the effect of the underlying hard-sphere core into account by the Shull *et al.* (1998) correction. The authors assumed the surface of the coated particle as a plane, in comparison with the dimensions of the penetrating sphere, to simplify the mathematical treatment. The adsorption layer is accepted as a homogeneous elastomer with an average thickness of h_0. Hertz theory relates the contact area of a penetrating sphere of radius R with the force through the bulk modulus of elasticity, K_{elb} [Nm^{-2}] related to the young's modulus of elasticity E through the poisson ration υ $\left[K_{elb} = \dfrac{3E}{(2(1-\upsilon^2))}\right]$:

$$F = \frac{K_{elb} a^3}{R} \tag{1.79}$$

where a is the radius of the contact area. The force applied by the colliding (penetrating) sphere, is shown in Figure 1.15(a). The penetrating body causes an indentation δ in the adsorbed layer proportional with the contact area:

$$\delta = \frac{a^2}{R} \tag{1.80}$$

The indentation can be related to the applied force through these equations by

$$F = K_{elb} R^{1/2} \delta^{3/2} \tag{1.81}$$

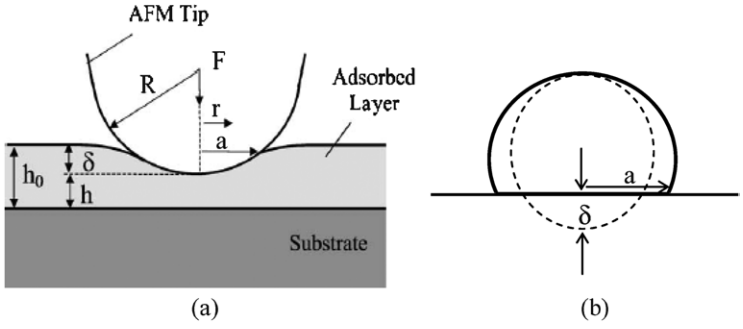

Figure 1.15 Dimensions related with deformabilities (a) of surfactant coating (Reproduced from Rabinovich *et al.*, 2004. Figure 2 in the original, with permission of Elsevier.); (b) of an elastic particle on interaction with a hard surface.

The indenting sphere causes the evolution of normal stresses within the elastomer film. The distribution of normal stresses $p(r)$ along the indenting sphere is given by Hertz theory as

$$p(r) = \frac{3K_{\text{elb}}a}{2\pi R}\left(1-\left(\frac{r}{a}\right)^2\right)^{1/2} \tag{1.82}$$

The pressure just when the sphere begins to indent into the adsorbed layer is the yield stress in the normal direction, Y:

$$Y = \frac{3F_Y}{2\pi a_Y^2} \tag{1.83}$$

where the subscript Y indicates the values of the variables at the yield point. The yield stress is associated with the "jump-in" value of the force as shown in Figure 1.14(b)–(c), where the force curve is interrupted at its maximum value and the distance suddenly drops to zero as the two surfaces adhere. Hertz theory is valid for low values of indentation, expressed as, $a/h_0 \ll 1$, after which the hard core beneath the elastomer film affects the stress distribution. This effect is taken into consideration by the Shull correction factors for the indentation

$$\delta = \delta_{\text{H}}\left(0.4+0.6\exp\left(\frac{-1.8a}{h_0}\right)\right) \tag{1.84}$$

and for the force assumed to act in a frictionless medium

$$F = F_{\text{H}}\left(1+0.15\left(\frac{a}{h_0}\right)^3\right) \tag{1.85}$$

where the subscripts H denote the values found by the Hertz equation. At low values of a/h_0 the indentation and force approach the Hertz values. Increasing values of a/h_0 cause an increase in the force created.

The yield stress Y bears significance as an indication of suspension stability. Rabinovich *et al.* (2004) showed that a linear relation exists between the yield stress and the number of carbon atoms in the alkyl chain of the adsorbed surfactants, the yield stress increasing linearly with the length of the chain. They also showed that the yield stress of adsorbed layers on hydrophobic surfaces and of layers with compact worm-like micelles to be greater than that of hydrophilic surfaces and spherical micelles, respectively, confirming the results of Grant *et al.* (2000).

1.8.1.2.1 Effect of particle deformability

In addition to the deformability of the adsorbed layers, the particle itself may also be deformable as in the case of polymer colloids, elastomers, and biological cells such as the red blood cells (RBCs). In such a case the contact area between the two particles becomes flattened by the repulsive force causing an increase in the contact area and hence the force, as shown in Figure 1.15(b). Vakarelski *et al.* (2003) analyzed the forces created in deformable bodies theoretically, backed up by experiments with AFM. They found that the critical force F_c necessary to destroy the adsorbed layers on deformable particles and to bring the surfaces into adhesive contact was ~10 times higher than that for the case of solid particles. If the force is below the critical force, the particles rebound and do not adhere. This result is significant in explaining the stability of deformable particles under variable forces, such as in the case of RBCs flowing in blood vessels of different diameters.

1.8.2 Stabilization by polymers and polyelectrolytes

Interactions of polymers and polyelectrolytes with particles were presented in Section 1.4.3 in connection with aggregation of particles. Steric forces brought about by adsorbed polymers can be used in stabilizing the suspensions. An advantage of steric stabilization is the possibility of complete coverage of the surface in maintaining the stability of particles. The disadvantage of this method is the difficulty in determining critical concentration of polymers at which the particle surfaces will be completely covered but the chains will be prevented from extending into the solution to avoid bridging between particles. Polyelectrolytes could also be used for steric stabilization. At pH values other than the isoelectric point of the polyelectrolytes, the stability will be maintained essentially by the steric repulsion between the functional groups of the polyelectrolytes. In this case, a thick adsorbed layer of polyelectrolytes will decrease the effect of van der Waals forces as well as the charge density on the particle, both helping the stabilization of the particles. The disadvantage of this method is that the repulsions between the charged layers will decrease at high ionic strengths making this procedure usable only under moderate strengths where DLVO theory is relevant.

An issue that is more challenging than the stability of individual particles is the stability of clusters within a narrow size range. This becomes a problem in the use of ferromagnetic nanoparticles in the high-gradient magnetic separation of proteins under high

ionic strengths. Particle clusters together with their adsorbed proteins should be above a definite size range to overcome the drag forces to be captured within the retention time in the separator. The difficulty of the situation lies in the control of the "start" and "stop" procedures for aggregation: It is easy to start the aggregation but very hard to stop it when a certain size range is reached and then ensuring that stability is maintained under all conditions prevalent in the environment of application. A comprehensive approach to the problem is reported recently by Ditsch *et al.* (2005) where magnetic particles of nanometer size range were subjected to partial coating by random copolymers of acrylic acid/styrene sulfonic acid/vinyl sulfonic acid (AA/SSA/VSA). By applying the polymers in amounts below that required for full coating, and adjusting the hydrophobicity by SSA and attachment density by AA, the cluster size could be kept under control. The authors found that the size and stability of the clusters could not be maintained by a single coating of polymer, no matter what the composition of the polymer or the ratio of polymer to particle is. Clusters of any desired charge or hydrophobicity could be made by applying the coating in two steps: First to proceed the clustering to the desired size range and the second to stabilize the already formed clusters. The critical parameters in the first coating were found to be the molecular weight of the polymer (denoted as the extent of polymerization, or number of repeating units, X_w) and the amount of polymer used. At low molecular weights of the polymer, coverage of the particles is not complete and large-sized clusters were formed under the action of van der Waals forces. As the molecular weight increased, better coating of the particles could be achieved and steric stabilization decreased the cluster size down to single primary particles. Bridging forces became dominant with further increase in the number of repeating units of polymer and caused the formation of clusters approximately two orders of magnitude larger than the size of primary particles. An example to the variation of the hydrodynamic diameter with the degree of polymerization is reproduced in Figure 1.16. The size of the clusters formed under the dominance of van der Waals forces were calculated for an energy barrier of $15k_BT$.

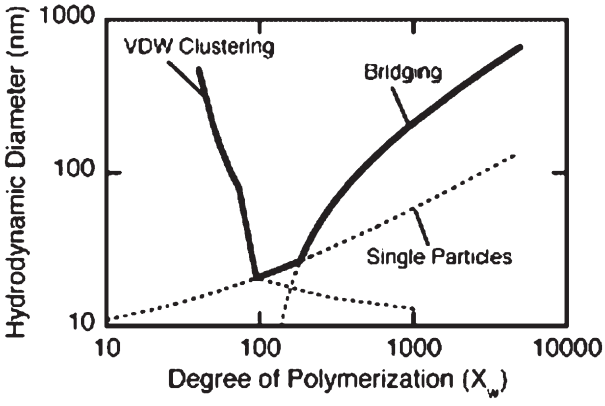

Figure 1.16 An example to the variation of cluster sizes with the degree of polymerization of the coating polymer (Reproduced from Ditsch *et al.*, 2005. Figure 11(a) in the original, with permission of American Chemical Society).

The three dotted-lined curves depict the variation of the hydrodynamic diameter of the cluster if only the represented force (i.e., van der Waals or bridging) were operative and the size of single particles sterically stabilized with a polymer of given molecular weight. The heavy line indicates the net effect, with the largest force controlling the hydraulic diameter for any given molecular weight of polymer used in the process. Contrary to low molecular weight polymers that produce particle-rich clusters, high molecular weight polymers were found to produce stable aggregates of bridged polymer networks low in solid particle content. Regardless of the charge of the hydrophilic group (cationic or anionic), all dimensionless diameters (diameter scaled to the minimum diameter) fell on the same curve at the same value of X_w/X_{min}, where X_{min}, is the number of repeating units in the polymer causing the formation of minimum diameter clusters. These results showed that hydrophobicity of the polymer chain is effective in determining the minimum number repeat units that should be present to minimize the diameter of the cluster and not the charge of the hydrophilic group. When limited amounts of polymer were used in the first stage of coating, the size of the clusters was found to reflect the relative rates of particle–particle aggregation and polymer–particle aggregation. Due to the insufficient amount of polymer used, the initially formed clusters are unstable. These clusters are stabilized soon after they are formed by a second polymer coating in amounts adequate to fill in the empty adsorption sites on the particle but not to cause bridging among the particles.

The authors (Ditsch *et al.*, 2005) modeled the aggregation process during the first stage of coating by the DLVO theory, using the Vold generalized van der Waals attractions applied to the polymer-coated materials:

$$-U_{vdw} = \frac{(H_m^{1/2} - H_c^{1/2})^2}{12} h\left(\frac{s-2\delta}{d+2\delta};1\right) + \frac{(H_c^{1/2} - H_p^{1/2})^2}{12} h\left(\frac{s}{d};1\right) + \frac{2(H_m^{1/2} - H_c^{1/2})(H_c^{1/2} - H_p^{1/2})}{12} h\left(\frac{s-\delta}{d};\frac{d+\delta}{d}\right) \tag{1.86}$$

This equation is a combination of eqs. (1.23), (1.24), and (1.25a) with R term nondimensionalized with the core diameter d; and separation distance s, scaled with the pertinent diameter, combined as an equation of the form:

$$h(s^*;R^*) = \frac{R^*}{s^{*2} + 2s^*R^* + s^*} + \frac{R^*}{s^{*2} + 2s^*R^* + s^* + R^*} + 2\ln\frac{s^{*2} + 2s^*R^* + s^*}{s^{*2} + 2s^*R^* + s^* + R^*} \tag{1.87}$$

where s^* and R^* are nondimensional distance and nondimensional diameter, respectively, the values of which are indicated in the functions of eq. (1.86). H_m, H_c, and H_p are the Hamaker constants for the medium, polymer coating and core particle, respectively. The other dimensions are shown in Figure 1.17.

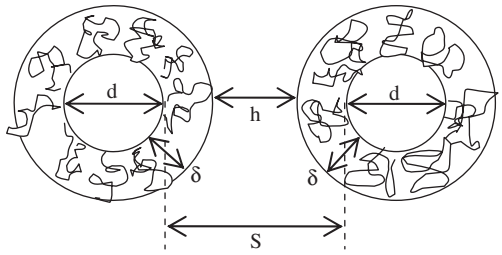

Figure 1.17 Dimensions of coated particles as used in eqs. (1.86)–(1.87).

The energy of repulsion between two coated spheres is estimated (Reiner and Radke, 1993) by

$$U_{\text{rep}} = 2\pi\varepsilon_r\varepsilon_0 r\,\Phi_0^2\,\frac{2}{2+(s-2\delta)/r}\exp[-\kappa(s-2\delta)] \tag{1.88}$$

The sum of eqs. (1.86) and (1.88) will give the total interaction potential between two particles. Vold and Vold (1983) gives the required energy barrier for stabilization to be at least 15 times the thermal energy, $15k_BT$. The required thickness of the polymer coating δ is estimated from the solution of eqs. (1.86) and (1.88). The height of the energy barrier in the resulting total interactive energy is a strong function of the ionic strength. Therefore, the authors suggest the employment of higher δ values than required for stabilization if the synthesized particles are to be used under higher ionic strengths. Typical value of the thickness δ is around twice the radius of gyration of the polymer (Aubouy and Raphael, 1998). As the radius of gyration of the polymer increases, the curvature of the particle limits the effective thickness of the layer.

The core size of the clusters are found (Ditsch *et al.*, 2005) from the rate of particle aggregation, and the cluster size d_{clus}, is related to the primary magnetic particle size d_c, by an equation similar to eq. (1.59):

$$d_{\text{clus}} = d_c\left(\frac{M_{\text{clus}}}{m}\right)^{1/d_f} + 4R_g \tag{1.89}$$

where M_{clus}/m is the number of primary magnetite particles in an average cluster, also called the *aggregation number* and d_f is the fractal dimension, for diffusion-limited colloidal aggregation. The thickness of the polymer coating around the cluster is approximated as twice the radius of gyration of the polymer, R_g, given by eq. (1.50).

1.8.3 Stabilization by nanoparticles

Another recent development involved the use of nanoparticles to stabilize the microparticles (Tohver *et al.*, 2001). As in the case of polyelectrolytes, surfaces of uncharged particles are energetically more favorable places for adsorption of charged nanoparticles.

Repulsions between microparticles coated with nanoparticle halos are essentially electrostatic in action. However, it also depends on the sizes of the nano- and microparticles and the ratio of their diameters, as well as on their volume fraction. Particle mixtures exhibit phase behavior much like their fluid counterparts. In a study of phase equilibrium among binary mixtures of different diameter particles (radius of nanoparticles = 3 nm and radii of microparticles either 285 or 590 nm), Tohver *et al.* (2001) found that a region of stability exists in between two gel phases, where the suspension acts like a fluid. This phenomenon was attributed to microspheres coated with charged nanoparticle halos. The phenomenon opens up many possibilities. Lee and Kramer (2004) used nanoparticle haloing to enhance self-assembly of colloidal crystals on patterned surfaces. Theoretical model studies of nanoparticle haloing (Karanikas and Louis, 2004) showed that halos are not a static layer of adsorbed particles, as in the case of steric stabilization. The nanoparticle halo is dilute and is in dynamic equilibrium with the bulk of the suspending fluid. A consequence of the dynamic nature of the halos is that stabilization cannot be maintained if the velocity of the microparticle is too fast for the nanoparticles to catch-up with. Nanoparticle haloing is a promising technology but needs further research for wide-scale application.

1.9 AGGREGATION IN BIOLOGICAL SYSTEMS

Aggregation takes place among living cells also: Aggregation in algae and microorganisms and subsequent sedimentation of the aggregates are responsible for the carbon cycle in the seas. Aggregation of microorganisms together with other inorganic colloids is desired in wastewater treatment. Reversible aggregation of red blood cells (RBCs) in blood regulates the retention time of these cells in various blood vessels through variations in viscosity, while irreversible aggregation of platelets help to repair injuries of the blood vessel wall even under high shear rates. The mechanisms that bring about aggregation of inorganic particles are also effective in the case of microorganisms. Two typical cases, blood cells and algae, will be taken up in this chapter as examples of cell aggregation.

1.9.1 Aggregation behavior of blood cells

Presence of blood cells, generally called *hematocrit*, give non-Newtonian characteristics to blood rheology through their aggregation and redispersion under the effect of shear. Hematocrit is mainly composed of RBCs, called *erythrocytes*, white blood cells (WBCs), called *leucocytes*, and platelets, called *thrombocytes*, at an approximate order of magnitude ratio of 10^6:10^3:10^5, respectively, in terms of number of cells per cubic millimeter. The liquid phase, *plasma*, is a solution of proteins (albumin, globulin, and fibrinogen), coagulation factors and electrolytes, mainly Na^+, K^+, and Ca^{2+}. Interaction and aggregation of blood cells are thus complex mechanisms involving electrostatic forces, van der Waals forces, surface forces related with polymers, and molecular recognition of receptors on another cell or colloid, all within a context of interrelated functions. As either aggregation or stabilization of the suspension is desired in various parts of the circulatory system in accordance with the function of the cells, the respective mechanisms must be in a

delicate balance. The mechanism of aggregation is determined by the requirement of these cells to perform their functions: RBCs are responsible for mass transfer of O_2, CO_2, and various nutrients and their consecutive transportation throughout the body. The velocity of the RBCs is reduced through aggregation under low shear rates to allow the required retention time for mass transfer. To speed up the transportation in between the sites of mass transfer, for example, to and from the lungs, the aggregates have to be broken up under high shear rates in the arteries and veins. In order to pass through narrow capillaries of diameter equal to their width they have to disaggregate into individual cells to be able to pass through. Therefore, the aggregation mechanism of RBC should be reversible, and be a function of the balance between attractive forces and shear stresses acting over the external surfaces. Platelets are mainly responsible for the repair of the damaged blood vessel walls, so the aggregates they form should be able to withstand the action of high shear rates. In addition, they should not form nonspecific aggregates with all the particles but only with those with which they can form a network for repair of the injured vessel wall. Therefore, aggregation based on molecular recognition of specific receptors is suitable with their function.

A water soluble protein, fibrinogen, plays a crucial role in the aggregation of all blood cells; therefore, its structure deserves special attention: Fibrinogen is an acute phase reactant whose concentration increases in times of injury to blood vessel walls, besides due to other factors. It is a glycoprotein with two symmetric parts, called D domains, each consisting of a set of three polypeptide chains denoted as $A\alpha$, $B\beta$, and γ, linked together by disulfide bridges which forms the central amino-terminal E domain of the elongated complex (MW = 340,000 Da). Adsorption to other entities take place only at specific sites at a specific orientation, i.e., there are sites on the D and E domains, which specifically bind to platelets, endothelial cells, thrombin, leukocytes or other blood components (Herrick *et al.*, 1999; Mosesson, 2000). Fibrinogen does not directly adhere to erythrocytes (RBCs) and also blocks erythrocyte–platelet aggregations. (Goel and Diamond, 2002). The self-association (D:D) sites are present at the two ends of the elongated molecule making possible the end-to-end linkages among the molecules (Mosesson, 2000). Thrombin generated upon vascular injury cleaves the complex molecule into fibrin and other cleavage products. The remaining fibrin monomers polymerise spontaneously and form insoluble fibrin clots after being cross-linked by transglutaminase (factor XIIIa) (Herrick *et al.*, 1999; Mosesson, 2000).

1.9.1.1 Aggregation of RBCs

Aggregation of RBCs is controlled by two factors: Their surface structure and their shape.

1.9.1.1.1 Surface structure of RBCs

A typical section of a cell membrane is given in Figure 1.18(a). A purely viscous phospholipid bilayer constitutes the cell wall of RBCs. Dispersed among the lipids are the membrane proteins with sialic acid residues suspended freely outside of this membrane. No receptor sites are reported in the literature for RBCs, so there are no specific adsorption sites for proteins and other molecules on the cell surface. Due to dissociation of the sialic acid groups, the surface bears a negative charge, with a surface charge density of

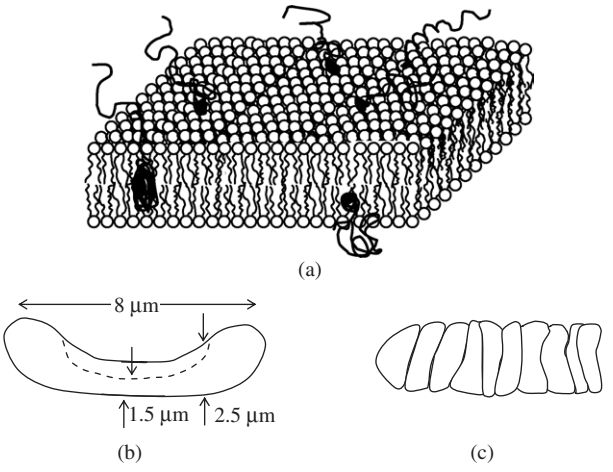

Figure 1.18 Red blood cells. (a) Surface structure, (b) shape and dimensions and (c) rouleaux formation in different sections of the circulatory system.

0.036 C m^{-2} (Vargas *et al.*, 1989; van Damme *et al.*, 1994). These charges are not fixed in space but are free to move together with the section of the polymer to which it is attached. The mobility of the hydrocarbon segments to which the sialic acids are attached cause the RBCs to act as soft particles instead of behaving as hard solid spheres. The average length of this section is around 5 nm which can be approximated as the width of the glycocalyx of an RBC. Debye length of the counterions is $\kappa^{-1} = 0.76$ nm (Neu and Meiselman, 2002). Viscoelasticity of the phospholipid membrane which resists expansion also contributes to the effect of the mobile glycocalyx on the aggregation mechanism.

1.9.1.1.2 Shape of the RBCs

The attractive forces, mainly van der Waals, between the hydrophilic and hydrophobic sections of the membrane lipids resist stretching during an increase in surface area upon deformation of the shape. A cytoskeleton made up of a network of proteins, mainly spectrin, is attached to the cell wall through interactions with membrane proteins. This protein network is responsible for the shape of the RBCs and the elasticity of the cell. The RBCs are elliptical concave discs of length equal to 8 μm and thickness 1.5 μm at the center and 2.5 μm around the circumference as sketched in Figure 1.18(b). The second centrally located concavity in the cell permits flexibility in cellular motion, making shape changes possible without an increase in surface area (Baskurt and Meiselman, 2003). These shape changes are required in the stacking of the aggregates, as well as orientation under shear forces to reduce drag.

Under the given conditions of surface structure and shape, interactions among RBCs are expected to be due to electrostatic charges, to van der Waals attractions and to the effect of polymers suspended in the plasma and integrated within the cell membrane.

1.9.1.1.3 Experimental observations of RBC aggregation

Ellipsoid disc shaped RBCs form stacks sketched in Figure 1.18(c), called rouleaux, when the shear rate is low. This aggregation is reversible, the rouleaux being dispersed into individual cells under high shear stresses. RBCs do not form aggregates in electrolyte (isotonic salt) solutions indicating the effect of repulsive electrostatic forces in the aggregation mechanism. It also indicates the role of polymers in bringing about the aggregation.

1.9.1.1.4 Effect of electrostatic charges

Erythrocytes, as other biological cells have a negative surface charge due to sialic acid end groups of glycoproteins located in the cell membrane. Sialic acid groups leave the cell wall with age or under the action of other molecules in the plasma such as trypsin and neuraminidase (Godin and Caprani, 1997). The surface charge density of normal and fresh erythrocytes is $-0.036\ \mathrm{Cm}^{-2}$. The negative surface charge on RBCs reduce the aggregation effect due to van der Waals forces and the bridging or depletion forces brought about by the polymers in the suspension medium (Armstrong *et al.*, 2004). This charge density decreases with the age of RBC, the decrease becoming more significant after 6 days. Cell rigidity accompanies the decrease in surface charge probably due to the modification of the integrated protein structure of the cell membrane, reducing the effect of viscoelasticity on cell repulsion and favoring aggregation.

The attractive and repulsive forces are important not only in the self-association of RBCs but also in their adherence to other surfaces, such as artificial organs. Measurement of forces between a RBC and a hydrophilic glass surface immersed in phosphate buffered saline with AFM (Luckham, 2004) showed the existence of repulsive forces at all interparticle separations. The repulsive interactions were found to become significant around 60 nm to the cell surface and increased very slowly as the cell surface was approached. A very strong repulsive force similar to the hydrophobic forces in inorganic systems was observed around 10 nm.

1.9.1.1.5 Effect of van der Waals forces

Attractive interactions of RBCs due to van der Waals forces were observed with hydrophobic surfaces by AFM (Luckham, 2004). When a glass surface was hydrophobized with silane, essentially replacing (–OH) groups with ($–CH_3$) groups, a minimum was observed at distances less than 100 nm, signifying the existence of attractive forces.

1.9.1.1.6 Effect of polymers

Polymers are present in blood in the form of proteins in plasma, or as sections of membrane proteins in the glycocalyx. Thus, steric, bridging, and depletion forces could all be effective in the polymer-mediated interactions. Steric forces evolve because of the repulsion between short-chain hydrocarbons adsorbed on particle surfaces. In the case of RBCs, the free end groups of polymers integrated into the cell membrane can create a repulsive steric force effect. However, due to high electrostatic repulsion, cell–cell distances at which minimal interaction energy occurs are always greater than twice the thickness of the cell's glycocalyx. Thus, steric interactions between glycocalyx on adjacent RBCs can be neglected (Neu and Meiselman, 2002).

Structures of plasma proteins are much more complicated than the nonionic polymers used in medical practices, such as dextran, and can be of various sizes and shapes. The most important plasma proteins in the order of decreasing concentration are albumin, globulin, immunoglobulins (IgA, IgG, and IgM) and fibrinogen. The presence of polymers suggests two possible mechanisms of aggregation: That of bridging through adsorbed polymers and that of depletion forces due to unadsorbed polymers. As explained above, bridging involves bonding of different cells together with the same polymer chain or direct bonding to polymers. To be able to form a bridge between different cells, the polymer should be long enough on expansion to span the distance between the cells. This rules out the short-chain polymers with low molecular weights and polymers with a spherical shape, such as immunoglobulins from bridge formation. Binding by depletion forces requires only the existence of an excluded volume in between the cells, on which the osmotic pressures act. As no bonds or polymer–particle interactions are involved in aggregation through depletion forces, it is relatively more reversible than aggregation through bridging which requires the simultaneous breakage of more than one bond on different cells. Armstrong *et al.* (2004) observed the molecular weight dependence of aggregation, when brought about by synthetic polymers, dextran, PVP and POE: Polymers with hydraulic radius less than 4 nm were either found to inhibit or not to affect the aggregation, whereas, polymers with hydraulic diameters greater than 4 nm were found to be strongly pro-aggregant. The aggregation effect was maximum in the range $6 \leq r_H \leq 12$nm, slightly greater than the size range of the RBC glycocalyx. Polymers of size, $r_H \geq 12$nm were found to deteriorate the aggregation of RBCs causing the formation of rounded and compressed clumps rather than elongated rouleaux (Armstrong *et al.*, 2004). Photographs taken *in vivo* by Pearson and Lipowski (2004) of rat RBCs flowing through a precapillary bifurcation after administration of fibrinogen (a) and Dextran 500 (b) are reproduced in Figure 3.14 in Chapter 3. Whereas, the rouleaux formed by fibrinogen cannot resist the shear under turbulent conditions existing at a bifurcation and tend to break up into irregular shapes, the rounded clumps formed by the action of Dextran 500 are quite stable. As the hydraulic radius r_H of Dextran 500 is 15.90 nm while that of fibrinogen is 10.95 nm (Armstrong *et al.*, 2004), the observed deterioration may perhaps be due to the effect of bridging bonds in addition to the action of depletion forces.

1.9.1.2 Aggregation of platelets

When a blood vessel is injured, the punctured endothelial cell lining of the vessel wall opens up, exposing the underlying extracellular cells. Disc shaped cells 1–4 μm in diameter, called platelets, are responsible for the control of bleeding (*hemostasis*) from these disrupted blood vessels. So they are equipped with receptor sites which selectively adhere to specific molecules on endothelial cells, collagen of the extra cellular matrix, other platelets, or on ligand complexes which form bridges between platelets and the cells to which they adhere. This selection mechanism, called *molecular recognition*, controls the adhesion to correct entities during the process of coagulation. Coagulation proceeds through the steps of molecular recognition, adhesion, signaling, activation of binding sites and final aggregation. Molecular recognition is carried out mainly by glycolipids (GP) acting as adhesion receptors embedded within the platelet membrane (Yip, *et al.*, 2005). Examples of adhesion receptors are GPVI that binds to collagen and GPIb-IX-V that binds

collagen-bound von Willebrand Factor (vWF). The latter, vWF, is an adhesive glycoprotein secreted by the platelets or endothelial cells into plasma or subendothelial matrix. Their very large size ($MW = 20 \times 10^6$ Da) and string-like shape facilitate the adhesion even under high shear rates observed in cases of high volumetric rates of blood flow. An argenine–glycine–aspartine (RGD) peptid sequence present in one of the subunits of vWF recognizes and strongly binds to an integrin in the platelet membrane, GPIIb/IIIa ($\alpha_{IIb}\beta_3$), responsible for strong aggregations with vWF, and similarly with fibrinogen. Because of the critical role played by the platelets in stopping blood flow, there are more than one mechanism (molecular pathways) for controlling blood flow, *in vivo*. However, at high shear rates above $\sim 650\,s^{-1}$ the pathway involving GPIb-IX-V becomes critical: A subunit of GPIb-IX-V in the platelet membrane, GPIbα, has a negative patch in its peptid sequence which strongly attracts a positive patch (A1) on vWF. The energy potential of this electrostatic attraction makes the adhesion resistant to shear forces.

When a plaque adherent on the interior lining of arteries is broken, a signal similar to vessel wall rupture may be transmitted to the platelets. This signal starts a similar procedure of aggregation of platelets within the internal cross section (lumen) of the blood vessel causing blockage of the vessel (*thrombosis*), observed in heart attacks and strokes, [Andrews and Berndt, 2004].

1.9.1.2.1 Prevention of blood coagulation

Ca^{2+} ions are closely involved in the aggregation of platelets and fibrin, through its effect on the activation of GPIIb/IIIa ($\alpha_{IIb}\beta_3$) (Guyton and Hall, 2006) and in the conversion of prethrombin to thrombin that converts fibrinogen into fibrin that enmesh the blood cells in forming the clot. Inhibition of coagulation is maintained by removing Ca^{2+} ions from the blood to decrease its concentration below the threshold level. This can be accomplished by precipitating the Ca^{2+} ions with *citrate* or *oxalate* anions.

Another way to inhibit coagulation is by addition of heparin to the blood. Heparin is normally present in blood, secreted by mast cells around capillaries where the probability of coagulation is highest due to slow rates of blood flow. When its concentration is increased, it forms a complex with antithrombin III, greatly increasing the effectiveness of the latter in removing thrombin and many other coagulation factors.

Still another way of preventing coagulation is through the addition of ethylenediamine tetracetic acid (EDTA). EDTA changes the shape of the platelets from discoids into spiny (thorny) spheres. The fibrinogen receptor located in the membrane matrix of the cells, GPIIb/IIIa ($\alpha_{IIb}\beta_3$) dissociates into its constituents, GPIIb and GPIIIa under the action of EDTA. The platelets exposed to EDTA lose their binding ability to fibrinogen with a decreased response to thrombin and collagen. As a result, clotting of blood is prevented. Recent studies show that this effect is reversible, and the platelets can bind to fibrins through which they can sustain clot retraction which necessitates tension development, even after being exposed to EDTA. The causes for this reversibility in the functions of EDTA are not clear as yet. Presence of GPIIb/IIIa deep in the glycocalyx matrix not reachable by EDTA molecules could be one reason (White, 2000), reassociation of GPIIb and GPIIIa be another, as well as another receptor such as an integrin assuming the functions of GPIIb/IIIa (Cohen *et al.*, 1989; Rooney *et al.*, 1998). The effect of EDTA on blood rheology will be discussed in Chapter 3.

1.9.2 Aggregation of microorganisms

Similar mechanisms, with some provisions, are operative in the aggregation of microorganisms including bacteria, algae, and yeasts. Aggregation processes include adhesion among microorganisms; between microorganisms and inorganic particles within a floc structure; and formation of microcolonies which develop into biofilms on solid surfaces. Aggregation of microorganisms to produce flocs involves a sequence of steps in the order:

1. weak reversible attraction, generally within the second energy minimum from the surface,
2. strengthening of the attraction through the excreted polymers to form a compact microaggregate of several cell diameters in characteristic dimension,
3. flocculation of these compact microaggregates in a loosely bound porous floc, generally described by the fractal theory.

The first step is sensitive to the ionic strength of the medium and takes place if attractive forces overcome the effect of electrostatic repulsion and shear forces when the suspension medium is in motion. DLVO theory should be used with caution in the case of microbial adhesion, taking into account the structural differences between inorganic particles and living microorganisms that have different capabilities. Pieterse and Cloot (1997) outlined these differences as:

1. The electrostatic charge distribution on a cell surface is not uniform. Overall, they are negatively charged but local positively charged sites cause specific orientations to be favored. Especially, if the microorganisms have fibrils that have positively charged areas along its length, attachment is maintained by the fibrils, even though the cell itself is negatively charged.
2. Microorganisms have irregular shapes. They have the ability to change their shapes to reduce the hydrodynamic resistance during motion.
3. Separation distance between cells is not well defined. As the length of the fibrils approaches the cell diameter in some microorganisms, the separation distance between the particles in the DLVO theory cannot be defined clearly.
4. Microorganisms with flagella can swim out of the flocs. Since the attractive forces in the second energy minimum are not strong, the living microorganisms can easily overcome these forces.
5. Gravitational forces may not be negligible. Gravitational forces, F_g, are of the same order of magnitude as the van der Waals forces for microorganisms of ~10–30 μm in diameter

$$F_g = G\frac{m_1 m_2}{s^2} \tag{1.90}$$

where G is the universal gravitational constant ($6.670 \times 10^{-11}\text{m}^3\text{kg}^{-1}\text{s}^{-2}$), m_1 and m_2 are the masses of two colliding bodies and s is the center-to-center distance ($s = h + R_1 + R_2$) between the bodies of radii R_i, and surface-to-surface separation h. Under the

action of gravitational forces the two microorganisms revolve around their common center of mass, facilitating aggregation.

6. *Mass transfer during photosynthesis can affect the hydrodynamics around the cell.* Algal cells assimilate CO_2 and other nutrients and excrete O_2 and organic molecules during photosynthesis. The net mass uptake perturbs the hydrodynamics in favor of flocculation. The photosynthetic pulling force, F_{ph}, can be approximated by

$$F_{\text{ph}} \approx \frac{3}{2}\frac{\pi\eta U r^4}{h^3} \tag{1.91}$$

where U is the mass up-take speed (m s^{-1}) and η, the viscosity of the suspension medium (Pa s)

7. Algal cells can react to perturbations in their environmental conditions. In case their charge is neutralized by the addition of flocculants to reduce the intercellular repulsion, the algal cells can react to re-establish their initial negative charge.

The second step in the floc formation involves the strengthening of the bonds formed by DLVO forces by the action of non-DLVO forces, generally exerted as bridging by polymers. These polymers could be provided by the cells as excretions or could be added as flocculants, as in the case of wastewater treatment (Chu and Lee, 2004).

The third stage of floc formation encountered in wastewater treatment processes involves other suspended solids and macromolecules to form irregularly shaped, fragile, highly porous and heterogeneous flocs (Chu and Lee, 2004). A minimum of two fractal dimensions, d_{f1} and d_{f2} were suggested to be used to describe the micro- and macrostructure of biological flocs: Wu *et al.* (2002) determined the fractal dimensions of sludge flocs by light scattering to elucidate the structure of the micro flocs of kaolin and activated sludge, presumably mixtures of kaolin and bacteria, captivated within macro clusters formed by a cationic polyelectrolyte. In the absence of polyelectrolytes, the fractal dimension of kaolin aggregates were $d_f \sim 2.0$, and those of activated sludges, $d_f \sim 2.12$, designating close-packed structures formed by electrostatic attractions. Addition of a cationic polyelectrolyte to the kaolin flocs caused a reduction in d_f, determined by light scattering down to DLA levels. Fractal dimensions of activated sludge clusters determined by free settling tests were much less, in the order of $d_f \sim 1.33$–1.48, denoting a loose, porous structure which controls the settling rate. In view of the fact that much smaller amounts of polymer are required for charge neutralization, the authors propose that the flocculation mechanism of activated sludge could be through bridging by polymers rather than charge neutralization of kaolinite.

REFERENCES

Adler, J.J., Singh, P.K., Patist, A., Rabinovic, Y.I., Shah, D.O., Moudgil, B.M., 2000. Correlation of particulate dispersion stability with the strength of self-assembled surfactant films. Langmuir, 16, 7255–7262.

Andrews, R.K., Berndt, M.C., 2004. Platelet physiology and thrombosis. Thrombosis Research, 114, 447–453.

Antalek, B., Williams, A.J., Texter, J., Feldman, Y., Garti, N., 1997. Microstructure analysis at the percolation threshold in reverse microemulsions. Colloids and Surfaces A: Physicochemical and Engineering Aspects, 128, 1–11.

Armstrong, J.K., Wenby, R.B., Meiselman, H.J., Fisher, T.C., 2004. The hydrodynamic radii of macromolecules and their effect on red blood cell aggregation. Biophysical Journal, 87, 4259–4270.

Aubouy, M., Raphael, E., 1998. Scaling description of a colloidal particle clothed with polymers. Macromolecules, 31, 4357–4363.

Baskurt, O.K., Meiselman, H.J., 2003. Blood rheology and hemodynamics. Seminars in Thrombosis and Hemostasis, 29, 435–450.

Bergstrom, L., 1997. Hamaker constants of inorganic materials. Advances in Colloid and Interface Science, 70, 125–169.

Berka, M., Rice, J.A., 2005. Relation between aggregation kinetics and the structure of kaolinite aggregates. Langmuir, 21, 1223–1229.

Berthon, S., Barbieri, O., Ehrburger-Dolle, F., Geissler, E., Achard, P., Bley, F., Hecht, A., Livet, F., Pajonk, G.M., Pinto, N., Rigacci, A., Rochas, C., 2001. DLS and SAXS investigations of organic gels and aerogels. Journal of Non-Crystalline Solids, 285, 154–161.

Biggs, S., Burns, J.L., Yan, Y., Jameson, G.J., Jenkins, P., 2000. Molecular weight dependence of the depletion interaction between silica surfaces in solutions of sodium poly(styrene sulfonate). Langmuir, 16, 9242–9248.

Birdi, K.S., 1993. Fractals in Chemistry, Geochemistry, and Biophysics, Plenum Press, New York.

Bordi, F., Cametti, C., Rouch, J., Sciortino, F., Tartaglia, P., 1996. Cluster formation in water-in-oil microemulsions at percolation: Evaluation of the electrical properties. Journal of Physics: Condensed Matter, 8, A19–A37.

Bouchama, F., Thathagar, M.B., Rothenberg, G., Turkenburg, D.H., Eiser, E., 2004. Self-assembly of a hexagonal phase of wormlike micelles containing metal nanoclusters, Langmuir, 20, 477–483.

Burns, J.L., Yan, Y., Jameson, G.J., Biggs, S., 1999. Relationship between interaction forces and the structural compactness of depletion flocculated colloids. Colloids and Surfaces A: Physicochemical and Engineering Aspects, 162, 265–277.

Burns, J.L., Yan, Y., Jameson, G.J., Biggs, S., 2002. The effect of molecular weight of nonadsorbing polymer on the structure of depletion-induced flocs. Journal of Colloid and Interface Science, 247, 24–32.

Chen, Q., Saltiel, C., Manickavasagam, S., Schadler, L.S., Siegel, R.W., Yang, H., 2004. Aggregation behavior of single-walled carbon nanotubes in dilute aqueous suspension. Journal of Colloid and Interface Science, 280, 91–97.

Chiavacci, L.A., Santilli, C.V., Pulcinelli, S.H., Bourgaux, C., Briois, V., 2004. Role of surface state and structural feature in the thermoreversible sol–gel transition of a zirconyl aqueous precursor modified by sulfuric acid. Chemistry of Materials, 16, 3995–4004.

Chu, C.P., Lee, D.J., 2004. Multiscale structures of biological flocs. Chemical Enginerering Science 59, 1875–1883.

Claesson, P.M., Poptoshev, E., Blomberg, E., Dedinaite, A., 2005. Polyelectrolyte-mediated surface interactions. Advances in Colloid and Interface Science, 114–115, 173–187.

Cohen, I., Burk, D.L., White, J.G., 1989. The effect of peptides and monoclonal antibodies that bind to platelet glycoprotein Ib-IIIa complex on the development of clot tension. Blood, 73, 1880–1887.

Derjaguin, B.V., Landau, L., 1941. Acta Physicochimica U.S.S.R., 14, 633.

Ditsch, A., Laibinis, P.E., Wang, D.I.C., Hatton, T.A., 2005. Controlled clustering and enhanced stability of polymer-coated magnetic nanoparticles. Langmuir, 21, 6006–6018.

Evans, E., Rawicz, W., 1990. Entropy-driven tension and bending elasticity in condensed-fluid membranes. Physical Review Letters, 64, 2094–2097.

Fleer, G.J., Scheutjens, J.M.H.M., Vincent, B., 1984. In: Polymer Adsorption and Dispersion Stability (eds. E.D. Goddard, B. Vincent), ACS Symposium Series 240, American Chemical Society, Washington, DC.

Fuchs, N., 1934. Über die Stabilitat und Aufladung der Aerosole. Zeitschrift fur Physik, 89, 736–743.

Godin, C., Caprani, A., 1997. Effect of blood storage on erythrocyte/wall interactions: Implications for surface charge and rigidity. European Biophysics Journal, 26, 175–182.

Goel, M.S., Diamond, S.,L., 2002. Adhesion of normal erythrocytes at depressed veneous shear rates to activated neutrophils, activated platelets, and fibrin polymerized from plasma. Blood. 100, 3797–3803.

Grant, L.M., Ederth, T., Tiberg, F., 2000. Influence of surface hydrophobicity on the layer properties of adsorbed non-ionic surfactants. Langmuir, 16, 2285–2291.

Guyton, A.C., Hall, J.E., 2006. Textbook of Medical Physiology, 11th edn., Elsevier Saunders, Philadelphia (Chapters 14 and 36).

Hamaker, H.C., 1937. The London van der Waals attraction between spherical particles. Physica, 4, 1058.

Helvacı, S., Peker, S., Özdemir, G., 2004. Effect of electrolytes on the surface behavior of rhamnolipids R1 and R2. Colloids and Surfaces B: Biointerfaces, 35, 225–233.

Herrick, S., Blanc-Brude, O., Gray, A., Laurent, G., 1999. Fibrinogen. The International Journal of Biochemistry and Cell Biology, 31, 741–746.

Hertz, H., 1986. Miscellaneous Papers, MacMillan, London.

Hoffmann, B., Köhler, W., 2003. Reversible light-induced cluster formation of magnetic colloids. Journal of Magnetism and Magnetic Materials, 262, 289–293.

Horng, H.E., Hong, C.Y., Yang, S.Y., Yang, H.C., 2001. Novel properties and applications in magnetic fluids. Journal of Physics and Chemistry of Solids, 62, 1749–1764.

Huang, A.Y., Berg, J.C., 2004. Aggregate restructuring by solvency effects. Journal of Colloid Interface and Science, 279, 440–446.

İkizler, B., 2005. Production of ZnO Nanoparticles Using Microemulsion Method. Master Thesis, Ege University.

Israelachvili, J.N., 1991. Intermolecular and Surface Forces, 2nd edn., Academic Press, London.

Israelachvili, J.N., Pashley, R.M., 1984. Journal of Colloid and Interface Science 98, 500–514.

Jönsson, B., Lindman, B., Holmberg, K., Kronberg, B., 1998. Surfactants and Polymers in Aqueous Solution, John Wiley and Sons, Chichester.

Jullien, R., Botet, R., 1987. Aggregation and Fractal Aggregates, World Scientific.

Karanikas, S., Louis, A.A., 2004. Dynamic colloidal stabilization by nanoparticle halos. Physical Review Letters, PRL93, 248303.

Kellner, R.R., Köhler, W., 2005. Short-time aggregation dynamics of reversible light-induced cluster formation in ferrofluids. Journal of Applied Physics, 97, 034910 (1–6).

Klokkenburg, M., Erné, B.H., 2006. Comparison of reversible and irreversible dipolar assemblies in a ferrofluid. Journal of Magnetism and Magnetic Materials, 306, 85–91.

Kuhn, H., Försterling, H-D., 1999. Principles of Physical Chemistry-Understanding Molecules, Molecular Assemblies, Supramolecular Machines. John Wiley and Sons Ltd., Madras, India (Chapters 13 and 14).

Kwok, R., Evans, E., 1981. Thermoelasticity of large lecithin bilayer vesicles. Biophysical Journal, 35, 637–652.

Lapasin, R., Grassi, M., Pricl, S., 1996. Rheological modeling of fractal and dense suspensions. The Chemical Engineering Journal and the Biochemical Engineering Journal, 64, 99–106.

Lee, C., Kramer, T.A., 2004. Prediction of three-dimensional properties of fractal aggregates. Advances in Colloid and Interface Science, 112, 49–57.

Letamendia, L., Louisor, E., Pru-Lestret, E., Rouch, J., Sciortino, F., Tartaglia, P., Ushiki, H., 1998. Relaxation phenomena in critical microemulsion systems. Colloids and Surfaces A: Physicochemical and Engineering Aspects, 140, 289–293.

Lifshitz, E.M., 1956. Soviet Physics JETP, 2, 73.

Lin, M.Y., Klein, R., Lindsay, H.M., Weitz, D.A., Ball, R.C., Meakin, P., 1990. The structure of fractal colloidal aggregates of finite extent. Journal of Colloid and Interface Science, 137, 263–280.

Lin, Q., Meyer, E.E., Tadmor, M., Israelachvili, J.N., Kuhl, T.L., 2005. Measurement of the long- and short-range hydrophobic attraction between surfactant-coated surfaces. Langmuir, 21, 251–255.

Luckham, P.F., 2004. Manipulating forces between surfaces: Applications in colloid science and biophysics. Advances in Colloid and Interface Science, 111, 29–47.

Mandelbrot, B.B., 1983. The Fractal Geometry of Nature, W.H. Freeman, New York.

Marsh, D., 1990. CRC Handbook of Lipid Bilayers, CRC Press, Boca Raton, FL.

Meakin, P., 1998. Fractals, Scaling and Growth Far From Equilibrium, Cambridge University Press.

Milling, A.J., 1996, Depletion and structuring of sodium poly (styrenesulfonate) at the silica-water interface. Journal of Physical Chemistry, 100, 8986–8993.

Milling, A.J., Vincent, B., 1997. Depletion forces between silica surfaces in solutions of poly (acrylic acid). Journal of the Chemical Society-Faraday Transactions, 17, 3179–3183.

Mohraz, A., Moler, D.B., Ziff, R.M., Solomon, M.J., 2004. Effect of monomer geometry on the fractal structure of colloidal rod aggregates. Physical Review Letters, 92, 155503, 1–4.

Mosesson, M.W., 2000. Fibrinogen functions and fibrin assembly. Fibrinolysis and Proteolysis, 14, 182–186.

Narine, S.S., Marangoni, A.G., 1999. Microscopic and rheological studies of fat crystal networks, Journal of Crystal Growth, 198/199, 1315–1319.

Neu, B., Meiselman, H.J., 2002, Depletion mediated red blood cell aggregation in polymer solutions. Biophysics Journal, 23, 2103–2109.

Özdemir, G., Peker, S., Helvacı, S., 2004. Effect of pH on the surface and interfacial behavior of rhamnolipids R1 and R2. Colloids and Surfaces A: Physicochemical Engineering Aspects, 234, 135–143.

Pearson, M. J., Lipowsky, H. H., 2004. Effect of fibrinogen on leukocyte margination and adhesion in postcappilary venules. Microcirculation, 11, 295–306.

Peker, S., 2006. Role of surface forces on the formation and stability of fractal structures. In: Colloid Stability-The Role of Surface Forces, Vol. 1 (ed. Th. Tadros), Weinheim, 73–97.

Peker, S., Helvacı, S., Özdemir, G., 2003. Interface-subphase interactions of rhamnolipids in aqueous rhamnose solutions. Langmuir, 19, 5838–5845.

Pham, K.N., Puertas, A.M., Bergenholtz, J., Egelhaaf, S.U., Moussaïd, A., Pusey, P.N., Schofield, A.B., Cates, M.E., Fuchs, M., Poon, W.C.K., 2002. Multiple glassy state in a simple model system. Science, 296, 104–106.

Pieterse, A.J.H., Cloot, A., 1997. Algal cells and coagulation, flocculation and sedimentation processes. Water Science and Technology, 36, 111–118.

Poon, W.C.K., 2002. The physics of a model colloid–polymer mixture. Journal of Physics: Condensed Matter, 14, R859–R880.

Rabinovich, Y.I., Kanicky, J.R., Pandey, S., Oskarsson, H., Holmberg, K., Moudgil, B.M., Shah, D.O., 2005. Self-assembled Gemini surfactant film-mediated dispersion stability. Journal of Colloid and Interface Science, 288, 583–590.

Rabinovich, Y.I., Vakarelski, I.U., Brown, S.C., Singh, P.K., Moudgil, B.M., 2004. Mechanical and thermodynamic properties of surfactant aggregates at the solid–liquid interface. Journal of Colloid and Interface Science, 270, 29–36.

Reid, C.E., 1990. Chemical Thermodynamics, Mc-Graw Hill, New York (Chapter 10).

Reiner, E.S., Radke, C.J., 1993. Double layer interactions between charge-regulated colloidal surfaces: Pair potentials for spherical particles bearing ionogenic surface groups. Advances in Colloid and Interface Science, 47, 59–147.

Rooney, M.M., Farrell, D.H., Van Hemel, B.M., de Groot, P.G., Ford, S.T., 1998. The contribution of the three hypothesized integrin binding sites in fibrinogen to platelet-mediated clot retraction. Blood, 92, 2374–2381.

Selomulya, C., Bushell, G., Amal, R., Waite, T.D., 2002. Aggregation mechanisms of latex of different particle sizes in a controlled shear environment. Langmuir, 18, 1974–1984.

Shah, S.A., Chen, Y.-L., Ramakrishnan, S., Schweizer, K.S., Zukoski, C.F., 2003. Microstructure of dense colloid-polymer suspensions and gels. Journal of Physics: Condensed Matter, 15, 4751–4778.

Shen, L., Stachowiak, A., Fateen, S.K., Laibinis, P.E., Hatton, T.A., 2001. Structure of alkanoic acid stabilized magnetic fluids. A small-angle neutron and light scattering analysis. Langmuir, 17, 288–299.

Shull, K.R., Dongchan, A., Chen, W.C., Flanigan, C.M., Crosby, A.J., 1998. Axisymmetric adhesion tests of soft materials. Macromolecular Chemistry and Physics, 199, 489–511.

Smoluchowski, M., 1917. Versuch Einer Mathematischen Theorie der Koagulations-Kinetik Kolloider Lösungen. Zeitschrift fur Physikalische Chemie, 92, 129.

Stokes, R.J., Evans, D.F., 1997. Fundamentals of Interfacial Engineering, Wiley-VCH, Inc., New York (Chapters 2, 4).

Takenaka, M., Kobayashi, T., Saijo, K., Tanaka, H., Iwase, N., Hashimoto, T., Takahashi, M., 2004. Comparison in fractal dimension between those obtained from structure factor and viscoelasticity of gel networks of 1,3:2,4-bis-*O*-(*p*-methylbenzylidene)-D-sorbitol in polystyrene melt at gel point. Journal of Chemical Physics, 121, 3323–3328.

Tirado-Miranda, M., Schmitt, A., Callejas-Fernandez, J., Fernandez-Barbero, A., 2003. Aggregation of protein coated colloidal particles: Interaction energy, cluster morphology, and aggregation kinetics. Journal of Chemical Physics, 119, 9251–9259.

Tohver, V., Chan, A., Sakurada, O., Lewis, J.A., 2001. Nanoparticle engineering of complex fluid behavior. Langmuir, 17, 8414–8421.

Vakarelski, I., Toritani, A., Nakayama, M., Higashitani, K., 2003. Effects of particle deformability on interaction between surfaces in solution.Langmuir, 19, 110–117.

Van Damme, M.-P.I., Tiglias, J., Nemat, N., Preston, B.N., 1994. Determination of the charge content at the surface of cells using a colloid titration technique. Analytical Biochemistry, 223, 62–70.

Vargas, F.F., Osorio, M.H., Ryan, U.S., De Jesus, M., 1989. Surface charge of endothelial cells estimated from electrophoretic mobility. Membrane Biochemistry 8, 221–227.

Verwey, E.J.W., Overbeek, J.Th.G., 1948. Theory of the Stability of Lyophobic Colloids, Elsevier, Amsterdam.

Vicsek, T., Fractal Growth Phenomena, 2nd edn., World Scientific, Singapore, 1999.

Vold, R.D., Vold, M.J., 1983. Colloid and Interface Chemistry, Addison-Wesley, London, 1983.

Wang, Z., Holm, C., Müller, H.W., 2002. Molecular dynamics study on the equilibrium magnetization properties and structure of ferrofluids. Physical Review E, 66, 021405, 1–13.

Wasan, D., Nikolov, A., Moudgil, B., 2005. Colloidal dispersions: Structure, stability and geometric confinement. Powder Technology, 153, 135–141.

White, J.G., 2000. EDTA-induced changes in platelet structure and function: Clot retraction. Platelet, 11, 49–55.

Wu, R.M., Lee, D.J., Waite, T.D., Guan, J., 2002. Multilevel structure of sludge flocs. Journal of Colloid and Interface Science, 252, 383–392.

Yip, J., Shen, Y., Berndt, M.C., Andrews, R.K., 2005. Primary platelet adhesion receptors. IUBMB Life, 57, 103–108.